DESIGN OF A PSEUDO-REAL TIME MICROWAVE IMAGING SYSTEM FOR CYLINDRICAL DIELECTRIC STRUCTURES

A THESIS IN ELECTRICAL ENGINEERING
Master of Science in Electrical Engineering

Presented to the faculty of the American University of Sharjah
College of Engineering
in partial fulfillment of
the requirements for the degree

MASTER OF SCIENCE

by
SOUDEH HEYADRI NASAB
B.S. 2009

Sharjah, UAE
May 2011

DESIGN OF A PSEUDO-REAL TIME MICROWAVE IMAGING SYSTEM FOR CYLINDRICAL DIELECTRIC STRUCTURES

Soudeh Heydari Nasab, Candidate for the Master of Science Degree

American University of Sharjah, 2011

ABSTRACT

In this thesis, the design and implementation of a pseudo-real time Microwave imaging system for cylindrical dielectric structures is investigated. Two different prototypes that have the same frequency of operation (7.5 GHz) but different receiving antenna shape and switching scheme were designed, fabricated and tested. The cylindrical retina was able to obtain an image from one third of a cylindrical structure while the single column retina, which has rotational capability, was able to create a 360^{o} view of the structure under test. Both imaging schemes were tested for different structures of various size and dielectric material and they were able to successfully detect the impurities. Furthermore, a comparison between the system of cylindrical retina and a planner microwave imaging system was made.

Most of the research conducted in field of microwave imaging focused on planner structures and was aimed to inspect the presence of inhomogeneities. Imaging of cylindrical object received some attention recently. However, very few attempts have been done to design an imaging system to specifically interrogate the integrity of cylindrical structures. This thesis specifically focuses on this area and the system offer novelty in terms of shape of retina and accuracy of distinguishing between materials of various dielectric constants. The scanning and switching stage designed for this project is also novel.

CONTENTS

LIST OF ILLUSTRATIONS

ACKNOWLEDGEMENTS

I take this opportunity with much pleasure to thank all the people who have helped me throughout my studies and particularly working on this thesis.

I have been indebted in the preparation of this thesis to my supervisors, Dr. Nasser Qaddoumi and Dr. Lutfi Albasha, who have been my supervisors since my undergraduate studies. Their patience and kindness, as well as their academic experience, have been invaluable to me. I feel so blessed for the chance of working with them.

I would like to extend my gratitude to Dr. Yousef Al-assaf, Dean of college of Engineering, for sincerely helping me in numerous ways all along my studies, without his support and understanding this thesis would not have been completed in the way that I hoped for. It has been an honor to study under his supervision.

I also wish to express my Appreciation to Dr. Mohammed El-Tarhuni, department head of Electrical Engineering, who always showed interest in my work and his sincere help and understanding has been of great value to me.

Moreover, I am thankful to all the lab instructors, and above all Engineer Ibrahim Abu Seif and Engineer M. Narayanan, for their help during fabrication of the prototype for this thesis.

My sincere thanks are extended to Engineer Mohammad Asefi, for being a great friend and collogue in the last four years of my studies. Working with him has been a great experience and I am truly grateful to him.

And above all, my utmost gratitude goes to my wonderful parents ; my ***Mother*** for her unconditional love and support throughout my life and my ***Father*** who is my greatest role model and who always believed in me even when I doubted myself. They are the pillars of my life and without them I would not have come so far. I am also thankful to my brothers, Behrooz and Behzad, who always give me the sense of responsibility and make me try to be a better person.

To my parents

Nasser Heydari Nasab & *Effat Izadkhah Kermani*

And

all the parents who put their children's needs and dreams ahead of their own

For all you have scarified for me, I am eternally grateful to you

CHAPTER 1

INTRODUCTION

This chapter will provide a brief overview of this thesis. It starts by presenting a brief history of Nondestructive Testing and Microwave imaging. It then proceeds to clarifying the problem statement and motivation. Finally, the chapter ends with describing the objective of this thesis and the thesis outline.

1.1 Non-destructive imaging, a brief history

Nondestructive assessment of different structures has been a subject of interest for many years. From a composite structure or part of a human body, the main challenge is to detect a possible problem without damaging the structure under investigation.

From the end of 19^{th} century (1896) when the X-ray was introduced, different imaging techniques have been invented. Magnetic Resonant Imaging (MRI), Computerized Axial Tomography (CT scan) and ultrasound imaging are few examples of such techniques[1]. All of these techniques have one common objective which is seeing the internal structure of an object; however, each has its own advantages and disadvantages. For instance, X-ray does not provide as much information as MRI but it is less expensive. Furthermore, in X-ray and CT scan the radiation is hazardous while MRI radiation and ultrasound are not [2]. However, ultrasound imaging provides lower resolution images compared to X-ray. Moreover, ultrasound suffers from high attenuation when applied to low density structures[3].

Compared to these techniques, microwave imaging, which is relatively recent, has many advantages such as high sensitivity to dielectric properties variation and even invisible factors such as temperature and ions concentration, [4]. Moreover, unlike ultrasound imaging scheme, it can travel through materials with low density[5].

As the name suggests, microwave imaging scheme is based on utilization of microwave signals as a source of illumination. Microwave signals start from 300MHz and extend to 300GHz. As can be seen in the spectrum of Figure 1.1, these signals have a wavelength in the range of 1m up to 1 mm.

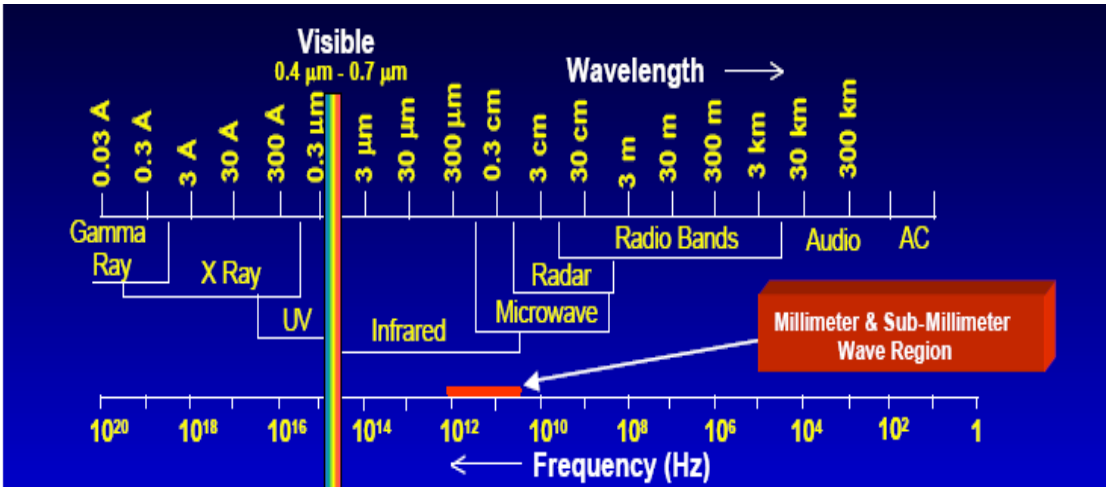

Figure 1.1: Electromagnetic spectrum [6]

Generally, a microwave image is obtained by illuminating the structure under investigation with a low power coherent microwave filed. An image is then generated by using the information gathered from the magnitude and phase of the scattered electric field by the structure[7]. The first hardware setup of an active microwave imaging system, made by Larsen and Jacobi in the late 1970s, was used to show the internal structure of a canine kidney. This experiment was performed using two antennas rotating around the object under test and the image was obtained by measuring the transmission coefficient between the antennas [8].

After Larsen and Jacobi's many researchers tried to develop other microwave imaging systems, however, these methods are application dependent. Thus several image reconstruction techniques have been developed as well.

1.2 Motivation and Problem Statement

As mentioned earlier, there are different methods of diagnostic imaging for medical applications; however, the nature of microwave signals and limitations of other systems due to different factors such as high cost (in systems such as MRI) and dangerous nature of adopted signals (in systems such as X-ray) increase the chance for microwave imaging systems. That is since microwave signals are less harmful and

have a potential of providing low cost diagnostic solutions. Furthermore, early stage detection of some particular diseases, such as cancer, is an important challenge considering the patient's life quality and survival chance. Such facts have increased the need for a high sensitivity and specificity diagnostic tools[9]. Microwave imaging can be considered as a successful solution in such cases. This is due to the fact that microwaves can directly provide a very detailed distribution map of the dielectric parameters while biological tissues present large variations in their electrical characteristics. For instance the contrast in permittivity for different tissues such as fat, bone, and malign tumour is quite notable[13]. That is while such information cannot be obtained using any other available imaging technology[9].

To contribute to early stage detection of some particular diseases, it was decided to concentrate this thesis on design and implementation of microwave imaging system that can be used in biomedical application. Since usually human body and organs are modelled and studied as cylindrical structures[10], it was also decided to choose a system suitable for scanning cylindrical structures. Thus, a prototype was designed to obtain images of cylindrical structures. The designed prototype can be used to develop a system for potential real life applications as well. Moreover, other specifications of the system such as the frequency of operation and scattering method were chosen based on the availability of testing tools and components.

Consequently, the frequency of operation for this system was decided to be 7.5 GHz, and the system is chosen to work based on an active transmission through topology. More detailed explanation on this topology is provided in the upcoming chapters.

1.3 Thesis Outline

The chapters to follow provide more detailed information on microwave imaging and illustrate the proposed thesis further.

Chapter 2: In this chapter, the necessary background information to understand the designed system is discussed. In the first section of this chapter, different microwave imaging topologies are

explained in detail. That is while the second section contains summary of some of the most referenced works that have been published in this filed.

Chapter 3: The proposed system and its parts are discussed in different sections of this chapter. Moreover, this chapter includes sections on the simulation and design procedure for the main parts of the proposed system. Furthermore, the decision making process is also explained in this chapter.

Chapter 4: This chapter contains the necessary information on prototype manufacturing and obtained results. It starts by providing some information on the manufacturing of the main parts of the system. It then precedes with analysis of the obtained test results for each prototype. This chapter also includes comparison between two different antenna arrays for cylindrical structures. Moreover, to further illustrate the advantages of these topologies as opposed to planner retina in imaging of cylindrical structures, a comparison between the proposed system and planner imaging system based on practical tests and results is presented.

Chapter 5: As the final chapter, this chapter provides a summary of findings and achievements of this thesis. Furthermore, a few suggestions for future development of the current work are discussed.

.

CHAPTER 2

BACKGROUND AND LITERATURE REVIEW

Microwave imaging systems can be studied from different aspects. It is not only the physical structure and hardware of these systems that makes them differ from one another, but also the image reconstruction methods and the kind of result that they generate can be used as a way to categorize these systems. In microwave imaging systems, these characteristics are decided by the shape and the dielectric characteristics of the structures under inspection. For instance, the system that is used for non-homogeneous structures has different characteristics from the one dealing with homogeneous structures in terms of image reconstruction techniques[9]. The same concept applies while dealing with live tissues as oppose to lifeless structures. These are what lead to selection of a specific frequency (or frequency range) and system configurations.

In this chapter, the necessary literature review for clarification of the objectives of this work is discussed. The chapter begins by providing some fundamental information about microwave imaging characteristics and topologies. This information is required to select an appropriate topology to serve the purpose of this work. The chapter then continues by providing a summary on some of the most referenced researches that have been developed in this field.

2.1 Microwave Imaging Topologies

In general, microwave imaging systems can be classified by three main categories first of which is the presence of an active source in the imaging system. If no active source is present the system is called passive. As for the active imaging method, two different scattering schemes can be adopted; forward or backward scattering. This determines whether the system images the structure under inspection by detecting the reflected scattered signals from it or by detecting the scattered signals transmitted through it. The other category defining the imaging scheme is when classifying a microwave imaging systems based on its retina shape. The last category which decides the type of a microwave imaging system is whether they are adopted as

near-field or far-field imaging systems. Detailed explanation of each category is provided in the following sections.

2.1.1 Active/Passive and Scattering Method

As mentioned earlier, the microwave imaging systems are classified into passive or active systems. The working principle of passive imaging is based on using an already existing source of energy as the source of illumination. For instance, the solar microwave radiations scattered from the earth's surface can be a utilized as a source of illumination which can contribute to the total power level detection. This method is mainly adopted in the sea, ice or snow mapping **Error! Reference source not ound.**. On the other hand, active microwave imaging is based on generating a signal of desired frequency as the source of illumination. This method is the most widely used microwave imaging scheme especially in near-field imaging of the objects. This type of imaging which is widely used in wide range of applications such as nondestructive testing, breast tumor detection would be discussed in section 2.1.3.

Furthermore, when it comes to active imaging scheme, two different types of images of the structure under investigation can be adopted. One of these schemes adopts forward scattered electric field and is also known as through transmission method. Using this scheme, the information about the structure to be imaged is gathered via a receiver sensor placed on one side of the object while the illumination source is placed on the other side. This scheme is further illustrated in Figure 2.1.

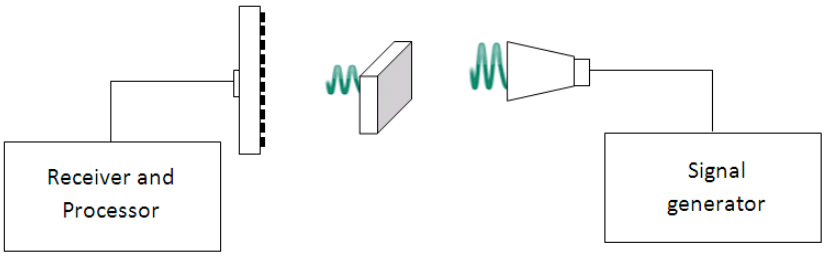

Figure 2.1 : Through transmission scheme

The other scheme of active imaging is based on utilization of reflected electric field from the structure under study which is known as the back scattered method or radar effect [1], [7]. In this scheme, both the illumination source and the receiving

sensor (antenna) are placed at one side of the object and based on different configurations, information about the structure under test can be gathered [12][13]. Figure 2.2 illustrates two different configurations of planner retinas that use the radar effect.

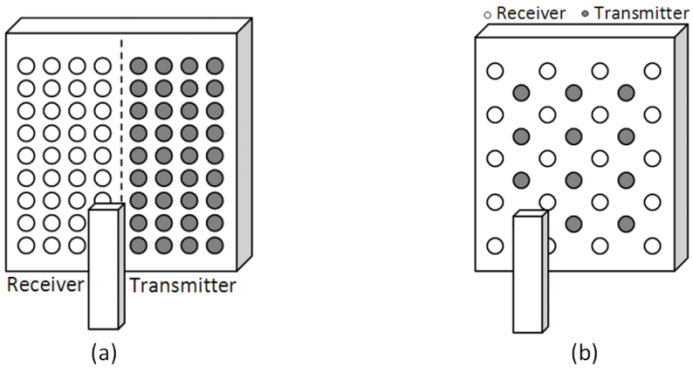

Figure 2.2 : Radar effect technique imaging (a) [13] , (b)[14]

2.1.2 Retina shape

Even though microwave imagers (camera) differ in term of their transmission and reception methods, they also differ in terms of their receiver shape since the structures to be imaged differ in their shape. The first type of early cameras was a planner microwave camera developed by Bolomey in Paris. It simply consisted of two horn antennas, one used as the transmitter and the other as the receiver collector, using the through transmission technique. Furthermore, to enable quick data acquisition, an array of 32 by 32 dipole antennas was placed in front of the receiver collector antenna [1],[15]. However, planner antenna arrays are not necessarily the best when it comes to imaging cylindrical objects. That is if, for instance, a planner receiving array was to be used as the receiving antenna for imaging of a cylindrical concrete column. In such scenario, other than the variations in phase and power level of the received signal, there will be different delays in the signal reception due to difference in spacing between the receiving array elements and different parts of the concrete column. This effect is further illustrated by Figure 2.3.

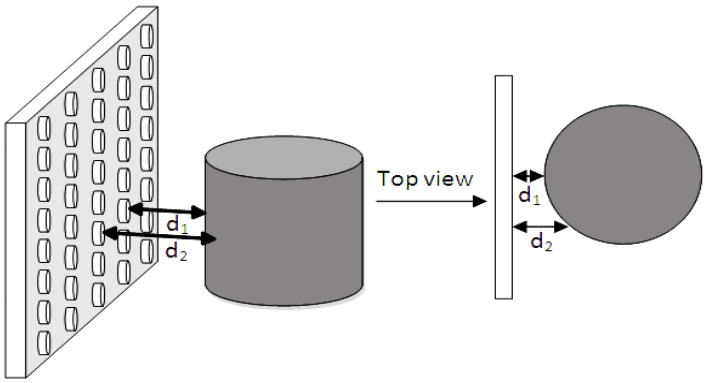

Figure 2.3 : The different spacing between the object points and the array

As can be seen from the diagram of Figure 2.3, d_1 and d_2 are not the same; thus, the processing of the data acquired by such a system will be more complex if not impossible in some scenarios. However, this problem can be solved if the imaging array is also cylindrical, providing the same spatial distance between the object and receiving array as illustrated by Figure 2.4.

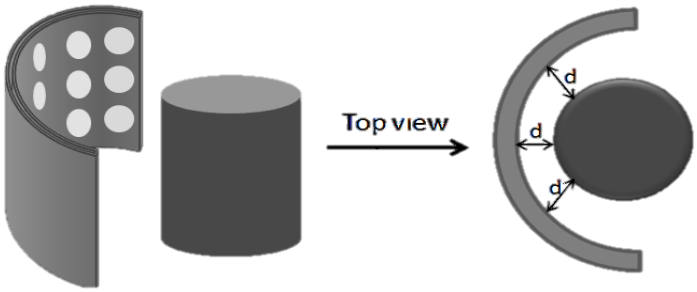

Figure 2.4 Equal spacing between the object and the cylindrical array

The first cylindrical scanner was introduced by Jofre et al. in 1990 in which a ring array was used to image an object (Figure 2.5) [10].

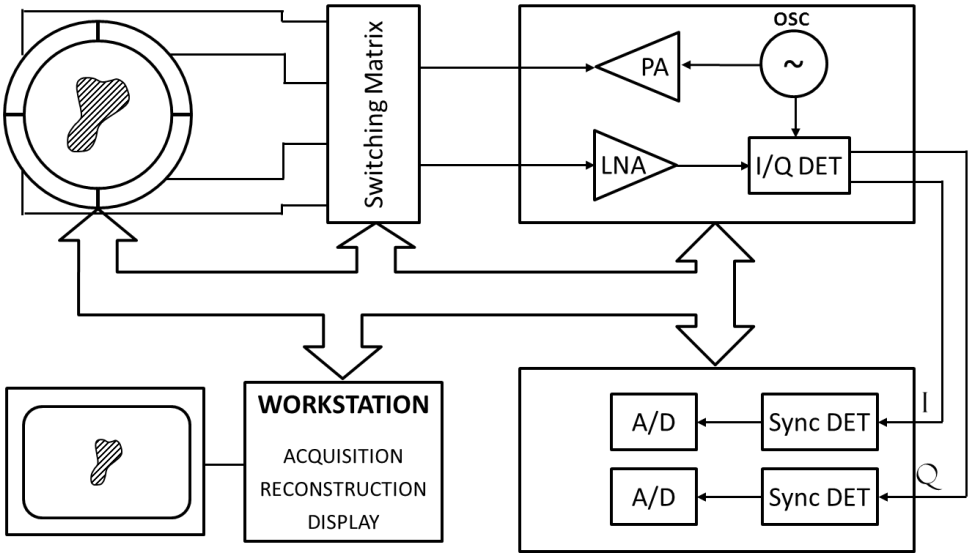

Figure 2.5 : Block diagram of the system [10]

The antenna array of this system consisted of 64 water loaded waveguides. As for data acquisition, one of the 64 antenna elements was addressed as the illuminating source (the emitter) while the half array elements in front of it worked as receiving sensors, scanning the scattered field from the object under inspection. This procedure was then repeated until one revolution (cycle) was completed. This system was tested for some medical applications and the results were impressing [7],[10].

Later on, in 1996, Semenov et al. developed a 64 element circular microwave imaging system using waveguide antennas as array elements. This system had 32 emitter and 32 receiver antennas operating at 2.45 GHz frequency. The antennas were located on the boundary of a cylindrical chamber filled with different solutions such as stilled water. This system was successfully used to reconstruct the image of a beating heart [16].

The developments and explorations on cylindrical microwave imaging methods were followed by Meaney et al. who developed a circular microwave imaging system for reconstruction of two dimensional electrical property distribution was developed [17], [18].

The most recent technology in this field is the millimeter wave scanners that are being used in some airports nowadays. These systems, known as Transportation Security Administration (TSA), began deploying state-of-the-art advanced imaging technologies in 2007. This technology is used to detect a wide range of threats to

transportation security in a matter of seconds to protect passengers and crews. These systems use two different types of imaging technology; millimeter wave and backscatterer. The backscatter technology projects low level (low power) X-ray beams over the body to create a reflection of the body displayed on the monitor while millimeter wave technology beams an RF signal on a person from two antennas that spin around the passenger at very fast speeds from head to toe. The energy reflected from the body and other objects generates a three-dimensional image of the passenger's body and anything else carried on the body of that person. Figure 2.6 and Figure 2.7 show some images obtained using millimeter wave and backscatterer systems respectively [19].

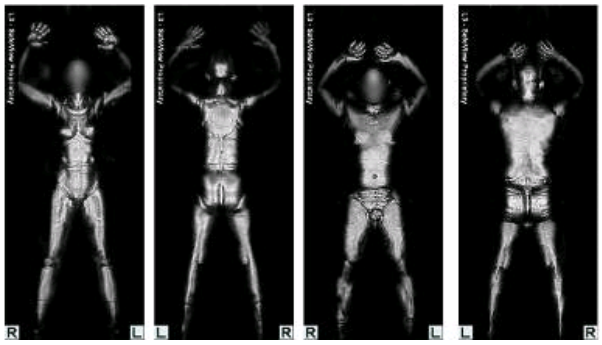

Figure 2.6 : Images obtained using millimeter wave system

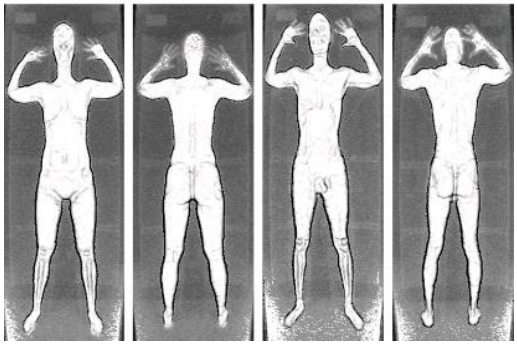

Figure 2.7 : Images obtained using back scatterrer

As can be seen from these images, the image obtained via the system adopting millimeter microwave signals is more detailed.

2.1.3 Near-field and far-field imaging

Another difference between microwave imaging systems is based on the distance of structure under inspection from the transmitting antenna which is

dependent on whether the system is designed for near-field or far filed imaging. These fields are defined based on the fact that along the radiation pattern of any antenna, there are three major areas, known respectively as reactive near-field, radiating near-field and far-field regions [20] as illustrated by Figure 2.7.

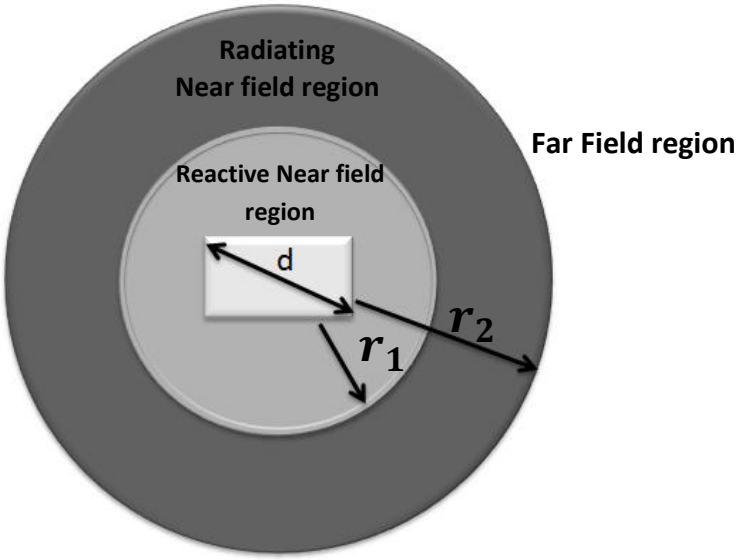

Figure 2.8 Field regions around an antenna

Reactive Near-field region is the portion of near-field region that starts immediately after the antenna. In this region, the reactive field dominates, meaning that the electric and magnetic fields are out of phase by 90 degrees [20],[21]. It is in this region where evanescent or near-field standing waves, which are known to have high frequency spatial information about the object of interest, exist[22][23]. On the other hand, radiating near-field, where the radiating fields begin to emerge, includes the region between the reactive near-field and the far-field region [20]. However, unlike the far-field region, here the shape of the radiation pattern may vary significantly with distance [21]. It is worth mentioning that if the maximum dimension of the antenna (d) compared to the wavelength of the transmitted signal is not large enough, this region might not exist at all. To calculate the radius of these two regions (r_1 and r_2), Equations (2.1), (2.2) and 2.3) can be used.

$$\lambda = \frac{C}{f} \tag{2.1}$$

$$r_1 \approx 0.62\sqrt{\frac{d^3}{\lambda}} \quad (2.2)$$

$$r_2 \approx \frac{2\,d^2}{\lambda} \quad 2.3)$$

where,

d is the largest dimension of the antenna,

λ is the wavelength of the signal,

r_1 is radius of the reactive region and

r_2 is radius of the radiating region

Far-field region of an antenna is defined as the region in which the radiating fields dominate. This means the electric and magnetic field planes are orthogonal to each other while the fields are in phase [20]. Moreover, in this region shape of the radiation pattern does not depend on the distance from the antenna [21].

These definitions can help understanding the basic difference between the far-field and near-field regions. Additionally, there are some other differences between these two types of imaging. For instance the antenna that is used in a typical near-field imaging system can be simple such as open-ended waveguide or coaxial line, while in far-field imaging, a high gain antenna should be adopted so that the signal would not disperse due to the distance [22]. Moreover, near-field imaging technique allows considerable enhancement of the power compared to far-field imaging with the same wavelength [24].

The other major difference between these two concerns is the spatial resolution of the image. As mentioned earlier, in the near-field region, the so called evanescence fields exist. However, by going further away from antenna these signals fade as they exist within a distance equal to the wavelength of the illuminating signal. Thus, they cannot be used in far-field imaging systems resulting in a lower spatial resolution for the images obtained via far-field imaging compared to an image obtained using near-field imaging. This is why in near-field imaging, more detailed image of the structure under test can be obtained[23],[25]. However, the main drawback of adopting near-field imaging is that the detector has to be placed near the

surface of the structure under inspection. As a result, near-field imaging is mainly thought of as a surface inspection technique and not as a nondestructive test method, although it has been used in that way [26]. Nevertheless, if the object of interest is larger than the wavelength of the illuminating signal, the far-field imaging is the natural solution. Furthermore, far-field imaging requires less complex image reconstruction algorithms compared to the near filed imaging due to the relationship between $\bar{E}$ and $\bar{H}$ fields in the near-field region.

2.2 Previously developed Microwave Imaging Systems

In the recent years, as a good non-ionizing method, microwave imaging proved to be a promising method for biomedical applications. The microwave images are basically maps of electrical property distributions in the body in which a change in these properties would be demonstrated as a contrast in the image. Thus, in cancer detection applications, for example, the cancer detection is due to differences in electrical properties between healthy and malignant tissues at microwave frequencies[27]. However, due to complexity of biomedical tissues, the wave propagation becomes more complicated. Additionally, in order to reconstruct an image with reasonable quality using microwave imaging, there is a need for high amount of calculations, which is due to the nonlinearity of scattering signals. Thus, in terms of hardware and software, these systems should have high sensitivity [1].

Previously, some of the works that has been done for development of microwave imaging systems has been briefly discussed in terms of their hardware specifications. Now, after providing some information regarding different classifications of microwave imaging, in this section a more detailed explanation of the developed schemes and their achievements will be presented. It is worth mentioning that the following works are only some among all that have been done.

2.2.1 THE PLANAR MICROWAVE CAMERA

As mentioned earlier, the very first microwave imaging system was developed by Bolomey et al. during the 80s. This work, shown in Figure 2.9, included two big horn antennas, with frequency of operation 2.45 GHz, and water tank in between. In this scheme, transmitter was designed so that it would roughly produce a plane wave that is received at the receiving side. The object had to be immersed in water, inside

the water tank, where scattered field due to the object was measured along a plane that was placed behind the object. Moreover, a retina of 1024 (32×32) elements, known as collector, was placed on the water tank in front of receiver. This retina is not considered to be the receiver but in terms of Modulated Scattering Technique (MST), its role is to disturb the field right before the receiving collector. By implementing this method, each antenna element is activated once at a time using a modulating signal of 200 KHz. That is while the received signal in collector provides data about the field properties of the antenna elements in that position. Therefore, scanning through all 1024 elements would provide a timely data acquisition with a rate of 15 images per second [28].

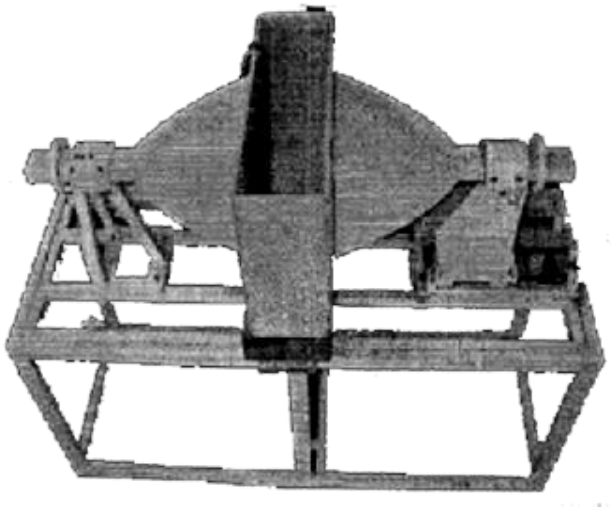

Figure 2.9 First Microwave imaging camera developed by Bolomey et al. 60[28]

2.2.2 THE 64 ANTENNA CIRCULAR MICROWAVE CAMERA

During the period when Bolomey's camera was going through its development, the first circular microwave camera (Figure 2.10) was developed by Jofre et al. This camera was able to perform multi view measurements without mechanical movements. The retina of this work, as it was briefly explained before, consisted of 64 horn antennas in a ring shape retina with diameter of 25 cm and operating frequency of 2.45 GHz. In this scheme, the antennas are used both as transmitter and receiver such that when one of them is transmitting, the others are receiving. This allows a rotational scanning around the object without actual mechanical rotation.

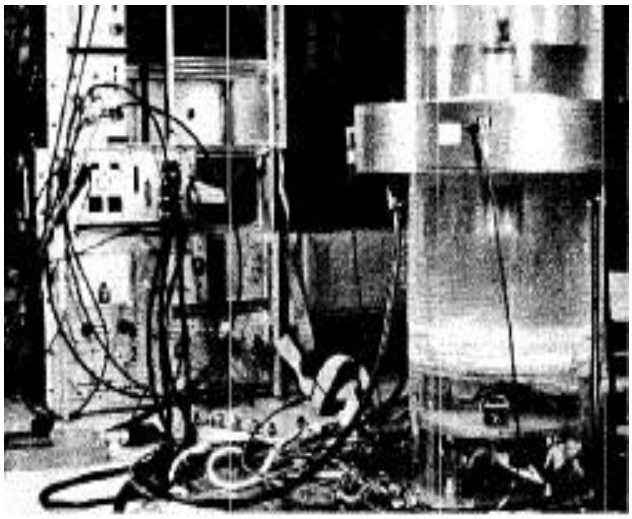

Figure 2.10 The circular microwave camera developed by Jofre et al. [10],[28]

In this work, antennas were divided into four 1-to-16 multiplexers, which are created by PIN diodes connected to the transmitter and receiver units. To decrease the leakage between the transmitting and receiving units, isolation was provided using a low frequency modulation in order to separate the useful signals from interferences [28].

This system was able to measure the object properties from 64 different angles around the object in 3 seconds; however, to reduce the noise effect averaging had to be performed and therefore a one cycle of measurements would take 45 seconds [29].

2.2.3 THE 32/32 ANTENNA CIRCULAR MICROWAVE SCANNER

A 64 element circular microwave scanner was developed by Semenov et. al.in mid 90's using waveguide antenna operating at a frequency of 2.45 GHz (Figure 2.11). This system was built to work based on principals of using antennas that could alternate between being a transmitter and receiver[30]. However, since this method suffered from a major isolation problem between the channels; antennas were divided in two groups of 32 elements, one as the receiving and the other as the transmitting unit. Nevertheless, this method has a drawback of having less number of possible inputs for the reconstruction algorithm as opposed to the scenario of using each single element as both transmitter and receiver.

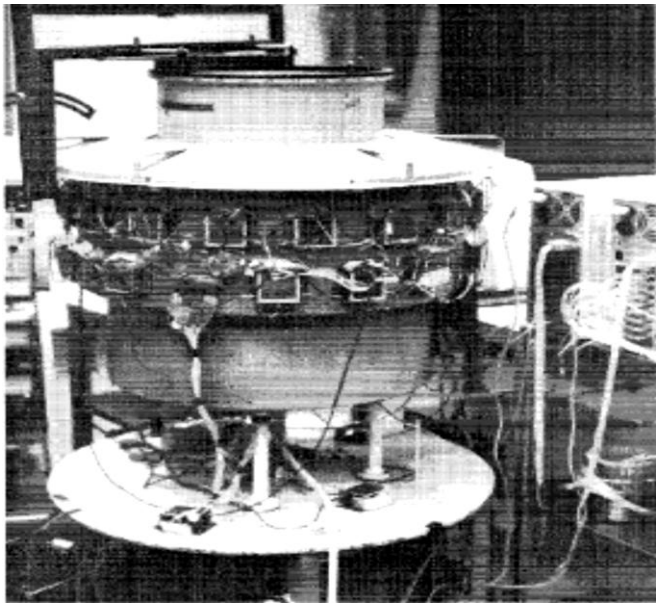

Figure 2.11 The circular microwave camera developed by Semenov et al.[30]

By means of this system, Semenov et al. were able to obtain an image of beating canine heart using data acquisition from all 32 transmitting and 32 receiving antennas around the object in less than 500ms.

2.2.4 THE CLINICAL CIRCULAR PROTOTYPE SCANNER FOR BIOLOGICAL IMAGING

In parallel with Semenov et al., Meaney et al. [17] were working on development of a circular microwave imaging system that could be used for reconstructing 2 dimensional electrical property distributions of objects. Initially, their system was composed of 8 waveguide antennas 4 of which were used as transmitters and the rest as receivers. The frequency of operation of their system was within the frequency range of 300 MHz to 1100 MHz so that by using multiple frequencies to find an optimal frequency. Also, by this mean the quality of the image could be improved due to the use of multiple frequencies and thus different penetrations[17].

Later on, in the late 90's this setup was further developed using a circular antenna array, with diameter of 25 cm, containing 32 monopole antenna elements. These antennas were used in both transmitting and receiving mode. (Figure 2.12)

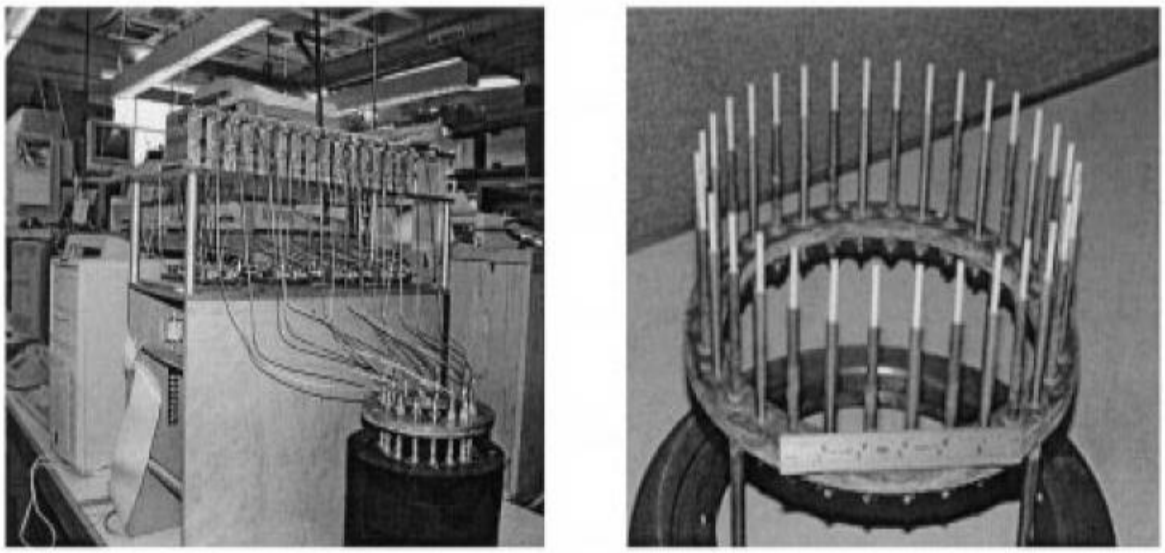

a) b)

Figure 2.12 The active microwave circular camera for imaging of biological materials, developed by Meaney et al. [17],[31] (a) The tank with the 32-channel data acquisition system (b) 32 monopole-antenna array

Even though the data acquisition method was the same as the older scheme, the overall results were improved. This was mainly due to use of monopole antennas which are easier to model as the group proposed. That is since, this antenna makes it possible to locate the object in the near-field region and still obtain acceptable field patterns inside the structure[31]. Conversely, waveguide antennas offer better gain but instead they need non-interfering space in near-field region. Meanwhile, using monopole antennas led to losses in SNR due to the low gain of monopole antennas. However, since this antenna allows minimizing the system around the object, some of the SNR losses could be regained as a result of shortening the distance between transmitter and receiver antennas.

Based on these experiments, Meaney et al. developed the first prototype of clinical active microwave imaging system for breast cancer detection in the early 21st century[18]. As can be seen in Figure 2.12, the system is mounted on a transportable bed with a hole for breast insertion. In this scheme, only 16 antennas in the antenna array with diameter 15cm are used. In this study, five real patients with different ages were involved and seven different frequencies were tested. The initial results were found to be sliced 2 Dimensional images of the breast with reasonable quality.

Figure 2.13 The clinical prototype for active microwave imaging of the breast developed by Meaney et al.[18]

In their most recent effort, Meaney et al. presented a new prototype working in the frequency band of 0.5 to 3GHz by which they have been able to produce images for breast cancer detection [32][1]. However, one of their main contributions to this field is considered to be the fact that an antenna as simple as monopole antenna, with wideband and simple model, can be used in biomedical application[1].

CHAPTER 3

Proposed system

The working sequence of the proposed system for this work can be summarized in few steps. First, using a sweep oscillator, a microwave signal of 7.5GHz frequency is generated and then radiated towards the structure under inspection by an antenna. Afterwards, this signal impinges on the desired structure and gets scattered. This scattered signal carries information about the structure under inspection. Thus, a receiving antenna placed at the other side of the object detects this scattered signal and transfers the result to a processing unit where the image of the structure gets reconstructed.

In this chapter, all the previously mentioned sections of the system are explained separately in detail. Furthermore, this chapter also includes simulation results for system elements that were specifically designed and made.

3.1 Frequency and Signal generation unit

As mentioned earlier, a sweep oscillator was used to generate a signal at a frequency of 7.5 GHz. This frequency was specifically selected due to limitations of the available instruments in the lab. However, this frequency is used as a proof of principle; later on, frequency of operation can be changed and the system can be slightly altered. Furthermore, this frequency is unoccupied which has the advantage of having no external interferers at this frequency.

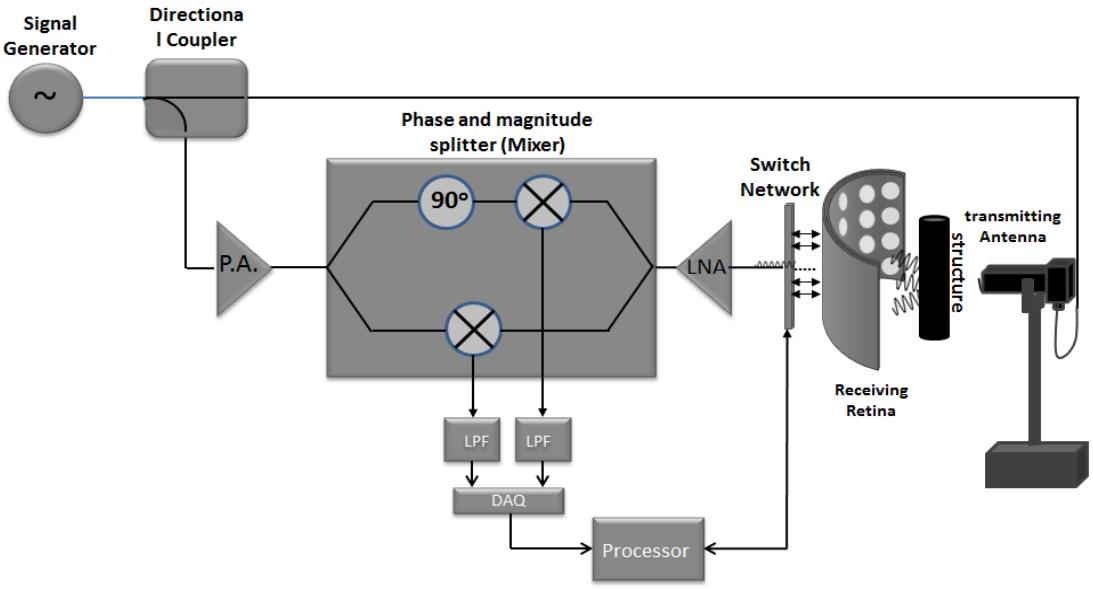

Figure 3.1 : The block diagram of the microwave camera

The signal generated by the sweep oscillator, as can be seen from the block diagram of Figure 3.1, has to be fed to a directional coupler. That is since part of the generated signal has to be transmitted via the transmitting antenna for illuminating the structure under inspection while a small portion of it is required as the reference for the down conversion unit.

3.2 Antenna

Selection and design of an appropriate antenna is one of the most important steps of this work and its design is dependent on many parameters. For instance, as for the transmitter, a single element antenna such as a W band (7.05 to 10 GHz) waveguide can be adopted. However, if a column of transmitting antennas is to be used, an array of waveguides can be bulky and expensive. Instead, as known for their ease of manufacturing, small size and low cost, an array of microstrip antennas can be designed. Yet, whether a pre-existing or a newly designed antenna is going to be used for the transmitter, it is not required to have the most optimized antenna. On the contrary, as for the receiver antenna; there are several considerations to be taken into account, the most important of which is the spacing between the array elements.

One of the main deciding factors in quality of an image is its resolution. The higher the resolution of an image is the more details it can provide about the structure it is representing. In microwave cameras, there are two main factors that can increase

the resolution of the image obtained. One of the deciding elements is the spacing between the receiver array elements. The smaller the spacing between them, the higher the resolution of the resulting image will be. However, this spacing cannot be reduced after a certain point since it introduces crosstalk (or mutual coupling) interference to the system. Crosstalk is generally a phenomenon by which a signal transmitted on one circuit or channel of a system creates an undesired effect in another circuit or channel and is usually caused by undesired capacitive, inductive, or conductive coupling from one circuit, an antenna element, or channel, to another. Yet, there are a few techniques and antenna designs by which this effect can be minimized up to a considerable extent.

The other factor that can improve the resolution of the obtained image is the size of the array elements which is decided mainly by the frequency of operation which in this thesis is decided to be 7.5 GHz. Thus, the frequency of operation becomes an initial design criterion.

However, designing an antenna array does not only require knowing the frequency of operation. The type of the antenna used is also as important. In this section, based on developments and results achieved by other groups in the field of microwave imaging, two major types of antennas are considered and studied for this thesis; circular patch and bowtie antenna both of which are microstrip patch antennas.

Microstrip patch antennas are mainly used in applications where size, weight, cost, performance and ease of installation are parts of the main criteria[20]. Moreover, these antennas are flexible to planner and non-planner surfaces, mechanically robust when mounted on a hard surface and flexible in terms of resonant frequency, input impedance, radiation pattern and polarization [20],[33],[34]. All these characteristics make this kind of antennas a good choice.

Among all shapes of microstrip patch antennas, circular patch is selected for this thesis. Meanwhile, bowtie antenna which is somehow categorized as dipole antennas is studied as well. This antenna could be considered for further developments of this work.

3.2.1 Circular patch antenna

Generally, circular patch antenna (Figure 3.2) is a better solution if used as a single antenna or a single column array since the control over mutual coupling is not very good in this configuration. However, this type is quiet easy to design and manufacture. As mentioned earlier, the main criteria to be considered for designing such an array is the size of the elements and their spacing. Moreover, the type and impedance of the feed used for this antenna is of importance.

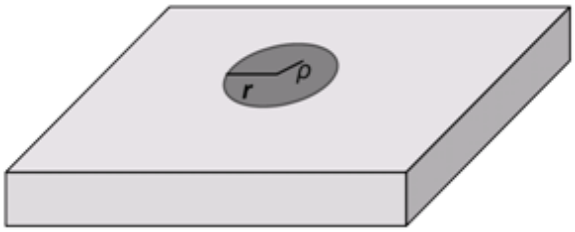

Figure 3.2: Circular patch antenna

In order to design this antenna, first, the radius of the patch should be calculated using Equations (3.1) and (3.2) [20].

$$r = \frac{F}{\sqrt{1+\frac{2h}{\pi\varepsilon_r F}\left[\ln\left(\frac{\pi F}{2h}\right)+1.7726\right]}} \tag{3.1}$$

$$F = \frac{8.791 \times 10^9}{f_r\sqrt{\varepsilon_r}} \tag{3.2}$$

where,
h is the substrate height,
ε_r is the substrate relative permittivity, and
f_r is the resonant frequency.

The resonant frequency of operation (f_r) was selected to be 7.5 GHz. However, as for the substrate, there are certain conditions to be considered while deciding on its type. Surface-wave excitation, dispersion of the dielectric constant, loss tangent of the

substrate and the copper cladding losses are some of the deciding factors. Additionally, since the retina of the proposed system has to be curved, some mechanical factors such as flexibility, ease of fabrication and soldering, , weight and elasticity become of importance .

Taking all the mentioned criteria into consideration, it was found that for 7.5 GHz, Rogers RT-duroid-5880 could be a reasonable choice. For this type of board, the substrate's relative permittivity (ε_r) and height (h) are given to be 2.44 and 0.787 mm respectively. Therefore, the physical radius of the circular patch can be found from Equation (3.1) to be 0.6898 cm.

Other than the physical radius, directivity is an important parameter that shows the ability of the antenna focusing radiated energy. The directivity of each element can be found 7.4352dB using Equation (3.3) [20].

$$D_0 = \frac{(K_0 r_{eff})^2}{120 G_{rad}} \tag{3.3}$$

where,

K_0 is the free space propagation constant ($\frac{2\pi}{\lambda}$),

r_{eff} is the effective radius of the antenna (Equation (3.4) -found to be to be 0.7995 cm)

G_{rad} is the radiation conductance of the antenna which is defined as conductance across the gap between the patch and the ground plane and can be found from Equation (3.5).

$$r_{eff} = r\sqrt{1 + \frac{2h}{\pi r \varepsilon_r}\left[\ln\left(\frac{\pi r}{2h}\right) + 1.7726\right]} \tag{3.4}$$

$$G_{rad} = \frac{\left(K_0 r_{eff}\right)^2}{480}\int_0^{\pi/2}\left[J_{02}'^2 + cos^2(\theta) J_{02}^2\right]\sin(\theta)\, d\theta \tag{3.5}$$

Furthermore, the radiation pattern of this single element circular patch antenna is presented in Figure 3.3. It should be noted that this graph is obtained using the MATLAB code provided in the part a of Appendix A.

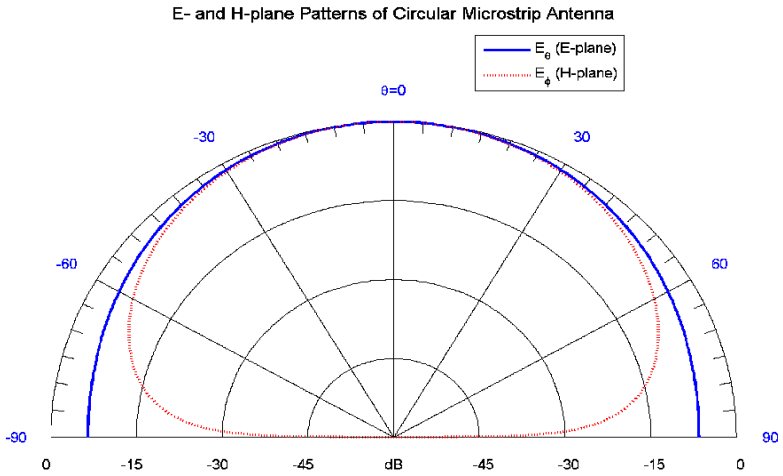

Figure 3.3: Radiation pattern of a circular antenna

Using this graph, the half power beamwidth (HPBW) of both electric field and magnetic field are found to be 92^o and 78^o respectively. Basically, the HPBW is the angle at which the power of the radiated signal drops by 3 dB.

As mentioned earlier, another important factor in design of a patch antenna is its feed location. Given the input impedance of the feed probe (R_{in}) and the effective area of the patch (a_e), the exact location of the feed (ρ) can be calculated through iterations using the Equation (3.6). This is done via the MATLAB code provided in Appendix A and the feed point was found to be ρ = 0.1758 cm.

$$R_{in(\rho'=\rho_0)} = \frac{1}{G_t}\frac{J_1^2(k\rho_0)}{J_1^2(ka_e)} \tag{3.6}$$

where

R_{in} is the input impedance (50 Ω),

a_e is the effective radius of the antenna,

G_t is the total conductance

Also, as for the distance between the elements, a simulation was run and the radiation patterns for three different spacing (d= λ, λ/2, λ/4) are shown in Figure 3.4

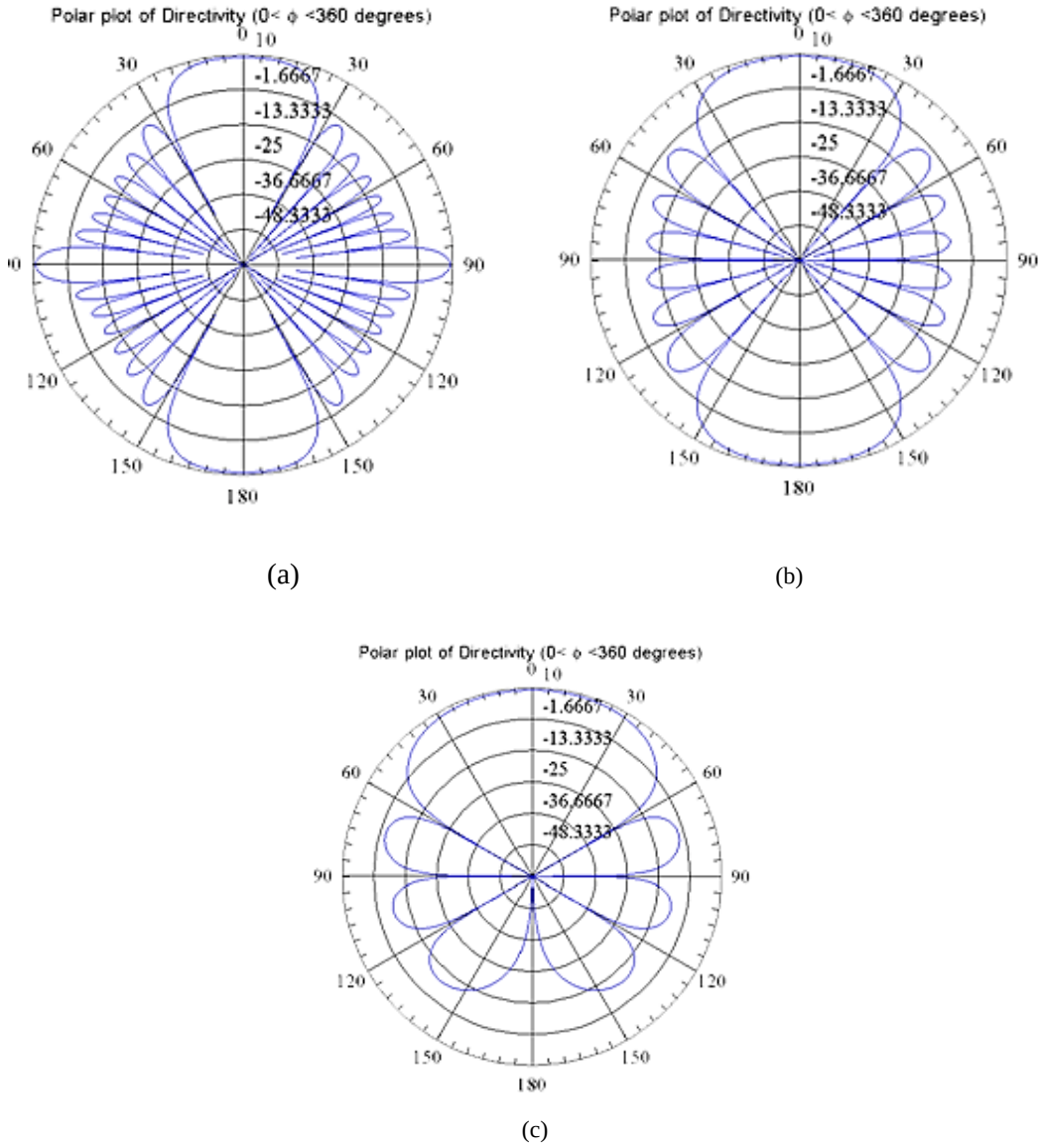

Figure 3.4: The array radiation pattern for spacing of (a) λ (b) λ/2 (c) λ/4

As can be seen from the radiation patterns of Figure 3.4, a decrease in the spacing between the array elements increases the half power beam width while it decreases the number of side lobes. However, after a certain point the radiation pattern is not desirable since the side lobes are going to get bigger and the HPBW is going to decrease drastically, thus, the minimum spacing can be λ/4.

Even though this antenna seems to have acceptable performance for the single column array; yet, its performance degrades if multiple column array antennas are adopted. That is since the crosstalk between the elements increases. Diagrams of Figure 3.5 represent possible crosstalk between antenna elements of a simple cylindrical shape retina.

a) b)

Figure 3.5 Crosstalk between retina elements in a cylindrical retina a) top view, b) front view

As can be seen from the top view of Figure 3.6 (a), compared to a planner shape retina of Figure 3.6, the cylindrical retina has increased crosstalk between elements due to the shape of the retina.

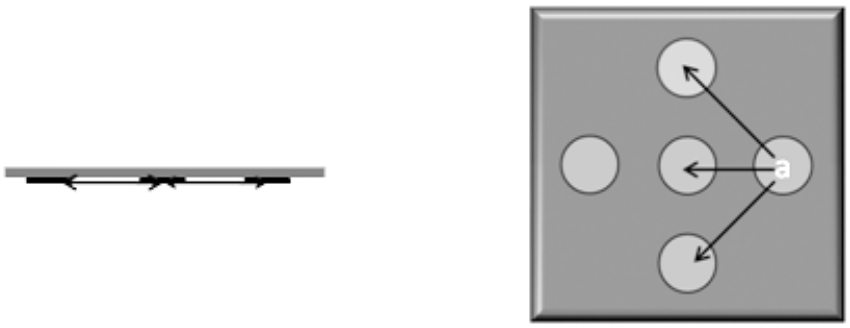

a) b)

Figure 3.6 Crosstalk between retina elements in a planner retina a) top view, b) front view

To decrease the crosstalk between array elements, the distance between them is set to the maximum possible. As mentioned earlier, it should be noted that increasing the array elements spacing results in a decrease of the system's resolution. Using the MATLAB code presented in part b of Appendix A, the most optimal distance between the array elements was selected. Figure 3.7 and Figure 3.8 represent the graphs obtained from this code. It is worth mentioning that each curve in these figures represents the cross talk due to a percentage of reflected power. The top curve represents a scenario in which the whole signal is reflected from the neighboring element(s) while the bottom curve represents minimum reflection.

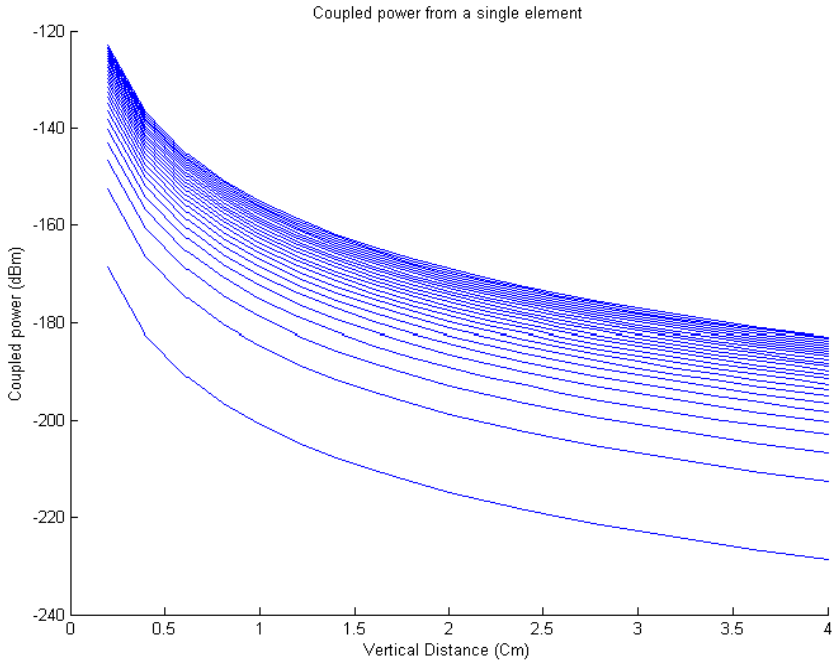

(a)

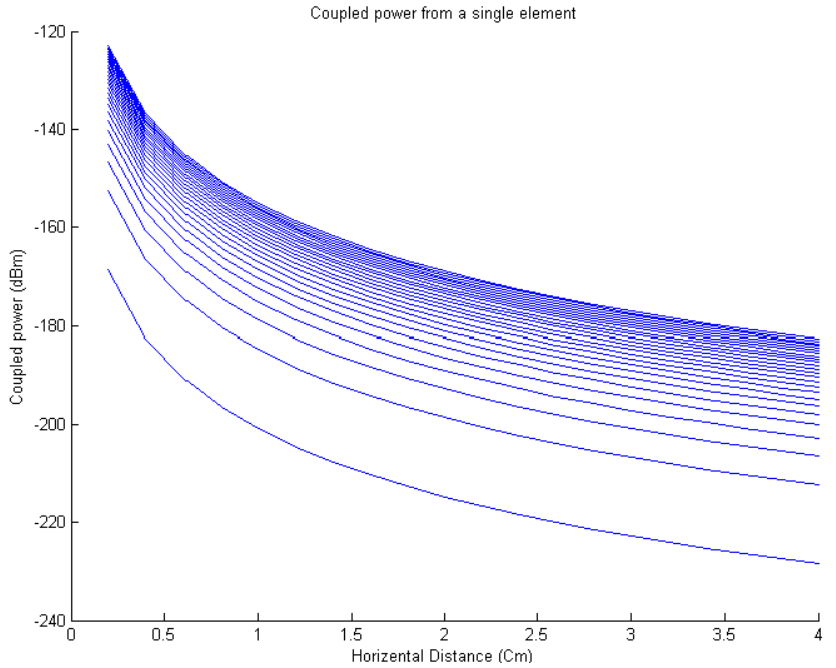

(b)

Figure 3.7 coupled power from two column (a) and row (b) elements in a cylindrical shape retina

Comparing these two figures, the coupled power from two elements in a row is slightly higher than that of two elements in column and this is due to the shape of the cylinder. However, to have a better estimate for the optimum distance between the antenna elements, the crosstalk effect between all neighboring elements has to be

taken into account. Figure 3.8 represents the graph that shows the cross talk from one tire of array elements.

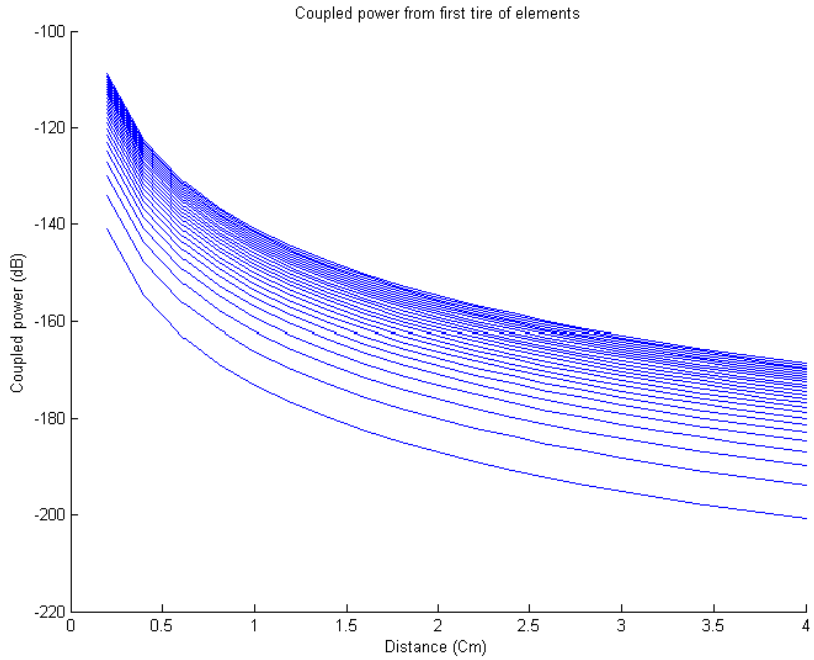

Figure 3.8 coupled power from the first tire of neighboring elements

Based on the results shown in Figure 3.8, it was decided to design the cylindrical retina for this project with element spacing of 2 cm. It should be mentioned that this distance could be future reduced to 1 cm; however, since the first prototype is done as a proof of principals, and in order to have minimal effects from neighboring elements, the 2 cm spacing was selected. This would cause the coupled power to be between -70 to -90 dB which is fairly tolerable for the proposed system.

To further reduce the effect of crosstalk between array elements, array elements are switched on one at a time. This is further explained in section four of the this chapter.

In addition to the issue of crosstalk, there are some other operational disadvantages concerning microstrip antennas. Some of these disadvantages are their low efficiency, low power, poor polarization purity, poor scan performance, spurious feed radiation and very narrow frequency bandwidth which is known to be the main disadvantage of conventional microstrip antennas[20]. In recent years, there have been many worldwide efforts in order to increase the bandwidth of these antennas.

Some of the suggested solutions includes increasing the substrate thickness, using antenna elements in multilayer geometry or in a planner gap configuration or cutting slots into the patch surface [32].Although these improvements in design specification can improve the bandwidth issue of the conventional microstrip antenna, one other way to take care of this issue is by using other type of antennas such as bowtie that can be classified as both microstrip and dipole antenna.

3.2.2 Bowtie antenna

Bowtie patch antenna (Figure 3.9), also known as triangular patch dipole, is simply composed of two flat triangular shaped metals on a dielectric substrate. As mentioned earlier, this type of antenna is best known for its broad bandwidth while maintaining the main characteristics of microstrip antennas such as low cost and small size. These characteristics make such antennas a good option for biomedical applications since in this field, in addition to having a small size, the antenna must be able to operate within a wide range of frequencies to achieve a high spatial resolution as well as suitable penetration of the field into the biological tissues[9].

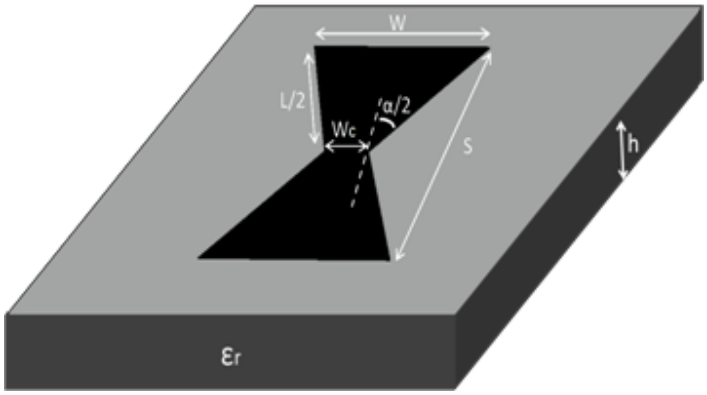

Figure 3.9 Bowtie antenna

Furthermore, another main reason that makes this kind of antenna appealing for microwave imaging is its capability to transmit and receive a relatively short pulse with minimal internal reflections. This characteristic is found to be useful while dealing with focusing effect since in such scenario instead of moving the transmitter, or the object, back and forth with respect to each other, the frequency could be changed such that the desired focusing effect is obtained [37]. This can enable the

system with the capability of layer scanning since the depth of penetration changes as the frequency alters. The equation of skin depth (Equation (3.7)) illustrates this effect further by showing the relation between the depth of penetration of a microwave signal into a material with respect to its frequency.

$$skin\ depth = \delta_s = \sqrt{\frac{2\rho}{2\pi f \mu_0 \mu_r}} \tag{3.7}$$

where,

ρ=bulk resistivity

f= frequency

μ_0 = permeability constant ($4\pi \times 10^{-7}$)

μ_r = relative permeability

For further illustration, Equation(3.7) was calculated at different frequencies and the graph of Figure 3.10 was obtained using matlab.

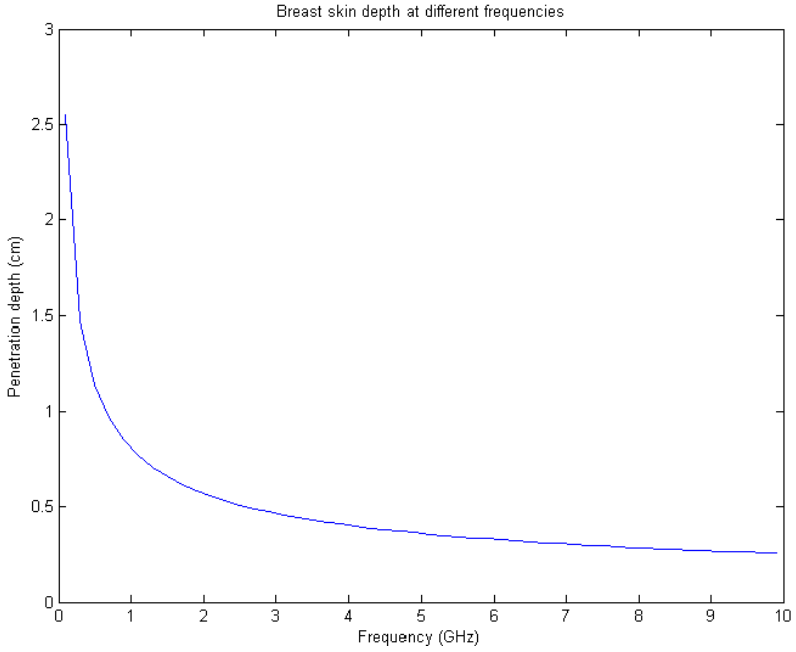

Figure 3.10 Breast skin depth at different frequencies

Even though in breast cancer detection, the maximum penetration is achieved at very low frequencies; yet, the resolution obtained at such frequencies would be quiet low due to the increase in physical size of the antenna by decreasing the frequency. Thus in most of the applications, signals with frequencies up to 7 GHz are used as the illumination source. However, the type and size of the antenna would

become a challenge at these frequencies since the smaller size can provide a higher resolution. That is since more antenna elements with smaller physical spacing can be adopted.

Additionally, bowtie antennas become even more appealing since their physical size can be further decreased by altering their designs such as using a double layered or loaded bowtie antenna. Although, the benefits of this type of antenna over other types of patch antennas, it has a few drawbacks the main of which is its design complexity.

In order to design a bowtie antenna, Equations (3.8) to (3.9) can be adopted. However, as can be seen from Figure 3.9 there are more unknowns than the Equations. This is one of the main challenges in designing this type of antennas.

$$f_r = 1.152\frac{C}{2\sqrt{\epsilon_{eff}}L}\frac{L}{2}\frac{[(W+2\Delta L)+(W_c+W\Delta L)]}{(W+2\Delta L)(S+2\Delta L)} \tag{3.8}$$

$$\Delta L = \frac{0.412h(\epsilon_{\text{eff}}+0.3)\left(\frac{\text{W}+\text{W}_\text{c}}{2\text{h}}+0.262\right)}{[(\epsilon_{\text{eff}}-0.258)\left(\frac{\text{W}+\text{W}_\text{c}}{2\text{h}}+0.813\right)} \tag{3.9}$$

$$\epsilon_{eff} = \frac{\epsilon_r+1}{2}+\frac{\epsilon_r-1}{2}\left(1+\frac{24h}{W+W_c}\right)^{-\frac{1}{2}} \tag{3.10}$$

where,

W_C is the width of the feeding neck
S is the height of the bowtie
f_r is the resonance frequency
h is the substrate thickness
ε_{eff} is the substrate's effective relative permittivity
ε_r is the substrate's relative permittivity
C is the speed of electromagnetic waves in free space

The common practice in designing such antennas is assuming the value of one variable while the others are found through iterations. Since bowtie equations are drawn from rectangular patch antennas, using the design equations of a rectangular patch antenna at the desired frequency can help in finding proper approximation for the value of W.

3.3 Retina

Retina, or basically what is known to be an array of antenna elements, is what serves as the receiving sensor in the proposed microwave imaging system. As mentioned earlier, the shape of the retina makes microwave imaging schemes different from one another. As for the proposed system, it was decided to focus on a system for imaging cylindrical shaped structures for which different imaging systems are proposed in this thesis. Each of these schemes has been studied and two of them were found to be the most applicable and practical ones were design, built and tested.

The first scheme adopts a cylindrical array of circular patch antenna elements. In this scenario, both backscattered and forward scattered methods could be implemented. Basically, back scattered design is when having a cylindrical retina where the transmitter and receiver both are placed in same side of the object under inspection, as shown in Figure 3.11. This mode of operation is also referred to as reflection back or radar method.

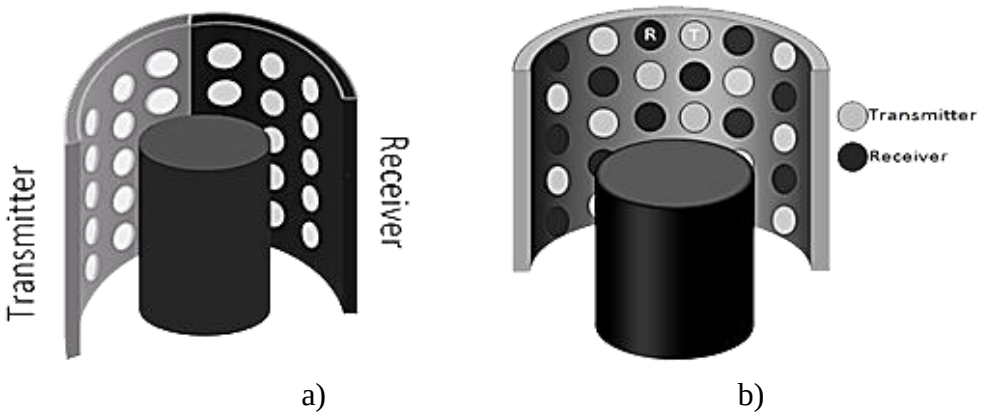

Figure 3.11: cylindrical array schematics for reflection method a) side-by-side receiver and transmitter b) mixed transmitter and receiver

However, when the transmitter and the receiver antennas are placed at opposite sides of the structure under inspection (Figure 3.12), forward scattering (or reflection through) mode can be achieved.

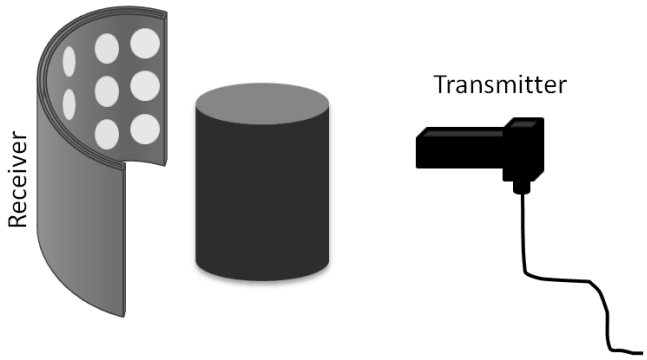

Figure 3.12 Cylindrical imaging scheme for scatter through technique

Although the shape of the receiving retina is the same in both methods; yet, switching a backscattered scheme is more complex compared to forward scattered scheme. Moreover, the antenna element crosstalk and the cost of switching for this scheme are other disadvantages that should be considered in designing a cylindrical shape retina.

These limitations led to design another type of microwave imaging system in which a single column of antennas is designed as the receiving retina. One of the main advantages of this system over the previously introduced one is the low number of antenna elements. Thus, the crosstalk from neighboring elements would be less. Furthermore, the number of required switches and therefore the overall cost of the system would be reduced as well.

To obtain a complete image of the structure under inspection, this system is required to have a motor so that either the antennas or the object are rotated 360o. To achieve this goal, two different system designs can be adopted as shown in Figure 3.13 and Figure 3.14.

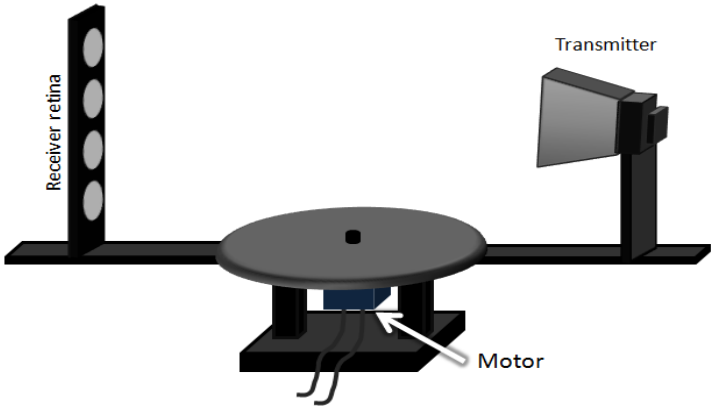

Figure 3.13 Single column receiver array with possibility of moving retina or object

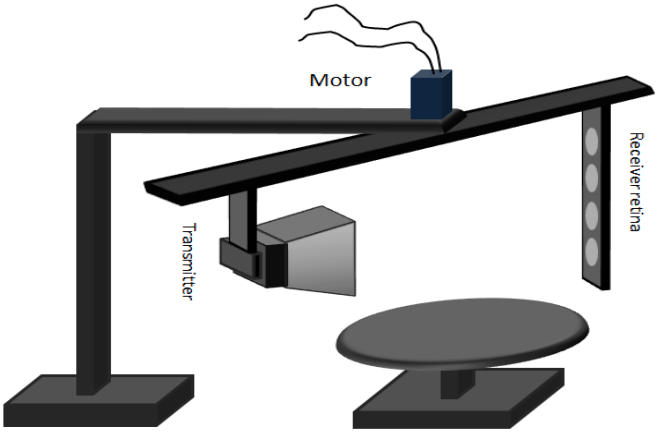

Figure 3.14 single column receiving array with moving retina

As can be seen from Figure 3.13 and Figure 3.14, the two systems are quiet similar and their main difference is the location of the structure under inspection. For instance, if an object is to be imaged, both systems can be adopted unless the height of the object is larger than that of the imaging system. In this case, the proposed system of Figure 3.13 would be preferable. However, for imaging parts of a human body, the imaging system of Figure 3.14 would be more desirable. Thus, despite the similarities of both designs, system of Figure 3.13 was selected for the prototype manufacturing and tests. That is since, at this stage of work, only non-biological structures are going to be imaged.

Even though this type of an imaging system has more advantages over the imaging system with cylindrical retina, yet it has some disadvantages as well. The main disadvantage of this system is its mechanical rotation which introduces a delay in updating the image obtained for an object. The optimization of the rotation and switching scheme are thus some of the main challenges of this design.

In addition to the rotational imaging system, the cylindrical retina was also designed so that the performance of each could be tested and analyzed practically.

3.4 The switching unit

Whether the imaging system with rotating antennas (or object) or the cylindrical retina is adopted as the imaging unit, a switching network is required to select antenna elements one by one. Thus, whenever a specific array element is selected using the switching network, the data gathered by that element would be transferred to the processing unit. In addition to acting as an address bus, the switching network can help in the reduction of crosstalk. That is since only one array element is activated at a time while others are switched off. The effect of crosstalk reduction using this scheme is more significant when the array elements are loaded [14].

To control switching between the receiver retina elements a matlab code was written to activate an element, get the data for that element and record it in a matrix. The elements of the matrix correspond to the image pixels. The main challenge of this part was writing a code that is optimized in terms of switching and recording speed and also in terms of switching method, i.e. whether the elements are activated one after the other or in a specific way. Moreover, since the imaging system used here consists of an array that corresponds to one third of a cylinder, the retina needs to be mechanically rotated around the object to be imaged to provide a 360^{o} image of the object. As mentioned earlier, this can be done via a motor. Thus, the switching should be repeated for each rotation step. The main challenge at this part will be providing the proper (or optimum) scanning (switching) scheme for the retina.

Matrix switches are the most flexible switching topologies through which it is possible to connect M row to N column of elements and turn on and off the elements in the manner that serves the objective better. These switches are known to have a very good isolation that can go up to 60dB. However, such switches are bulky and very expensive. On the other hand, conectorized SPnT, for this design SP6T (Figure 3.15), switches can also provide high isolation along with low insertion loss. However, since the retina for this work is designed to be an array of 6×6 antennas, in order to provide the switching between the elements using SP6T switches, 7 pieces of such switches would be required. Therefore, this solution is considered as an expensive alternative as well.

Figure 3.15 Typical connectorized SP6T switch

Thus, it was decided to design and fabricate a switching scheme that does not require any connectorized RF switches. This was done by using IC switches on a designed test PCB.

The designed switch networks contain three main components as shown in Figure 3.16; the IC switches which are HMC321LP4E switches manufactured by Hittite company;, RF capacitors that are used as bypass capacitor in order to remove the DC part of the signal; and SMA connectors to connect the switches to antennas and the DAC.

Figure 3.16 components for switches, from left to right; RFIC switch, RF capacitor, SMA connector

Furthermore, the designed PCB layout for the proposed switches is as shown in Figure 3.17.

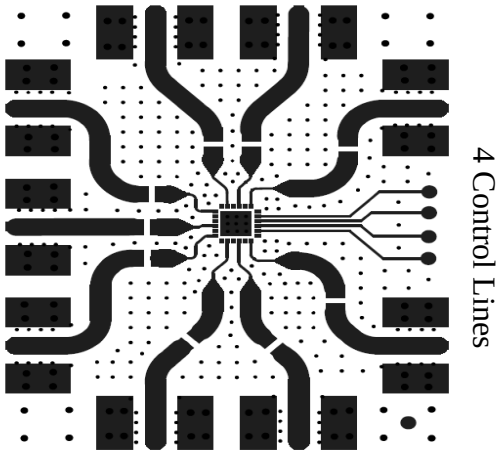

Figure 3.17 PCB layout for SP8T switches

3.5 The down conversion unit

The received signal from the switches needs to be fed to a data acquisition card so that it can be transferred to the processing unit for further analysis. However, the frequency of the signal is very high and it cannot be sampled at that frequency. Thus, it will be first amplified because of its low power and then fed to a down conversion unit which is an IQ mixer. The local oscillator (LO) of the IQ mixer is excited by the signal taken from the coupling arm of the directional coupler after amplification, that is to bring the low power signal to a level that can activate the mixer's LO. The reason for using an IQ mixer is that, this way, the information about both the phase and magnitude of the scattered signal can be extracted and used. If a simple mixing of this signal with the LO was done, a real DC signal will be generated which causes loss of most of the data. However, use of an IQ mixer provides a complex DC signal contains magnitude and phase information about the signal scattered from the object. The IQ mixer generates harmonics of the signal at higher frequencies. This can be solved by use of a narrowband low pass filter or a simple RC circuit at the output of I and Q ports of the mixer.

3.6 The processing unit

The low pass filtered signal will then be fed to a National Instruments data acquisition card which will be used as the interface between the imaging system and the processing unit. Afterwards, MATLAB is used to analyze the data and generate an

image of the structure under inspection. The MATLAB code developed for this part contains four main parts; a switching section, data acquisition section, a mechanical rotation section in case of the rotational system, and an image processing section. It is worth mentioning that the switching and mechanical rotation sections of this code are dependent on the scenario that will be chosen for the retina design.

3.6.1 Image processing

In this part, the data provided by the data acquisition card (DAC) is processed and displayed. Moreover, some image enhancement techniques can be applied to improve the quality of the image obtained. There are two methods of showing the desired image. This data can be either stored for all antenna elements and then processed, which provides an offline image, or it can be processed and shown as it is received in MATLAB for each element, providing a real-time updated image.

Moreover, in the image processing section, the effect of differences in soldering and length of cables should be taken into account so that the reproduced image becomes visually sensible. This is referred to as system calibration.

3.6.2 Image reconstruction mathematical modelling

Tomography is imaging the internal structure of any solid object by sections or sectioning, using waves of energy [38]. The main goal is to reconstruct an image from its diffracted projection meaning that the information derived from transmitted energies can be used, while an object is illuminated from an angle [39].

There are different mathematical algorithms, known as reconstruction algorithms, which can model the reconstruction procedure of a picture from its projections. These models mainly contain different approximations and are complicated, but in the case where implementation is not easy or possible these models are useful. In this research, although the microwave imaging system is going to be implemented, an overview of a possible algorithm is mentioned in Appendix C.

CHAPTER 4

Prototype and Practical Results

In this chapter, detailed information on the fabrication and calibration of the prototype of the proposed microwave imaging system are presented. The chapter starts by providing information on each part of the overall system separately. It will then end by presenting the results obtained for the designed imaging systems. In this section, detailed analyses of the images obtained via the proposed systems are presented. Additionally, the section includes a comparison between the results obtained from imaging specific structures using the proposed cylindrical imaging system and a planner imaging system.

4.1 Antenna

Since the receiver retina was supposed to have circular patch antenna elements, its fabrication was done using chemical process. That is since chemical PCB printing process provides features such as speed, accuracy, availability and low cost. Based on the theoretical designed parameters of the antenna found in Chapter 3, a layout was made on a transparent paper so that the layout could be imaged on the PCB. Then the antenna array was made through chemical development and etching process (Figure 4.1). Afterwards, the array elements were drilled at their feed location where the coaxial cables were soldered.

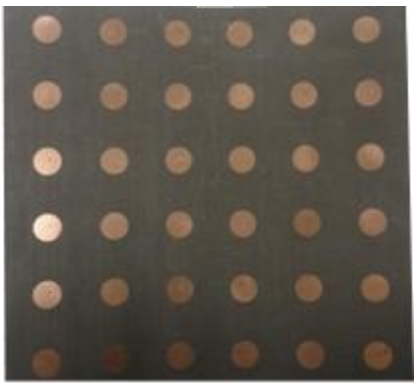

Figure 4.1 Array of 36 elements (6×6)

The soldering process was considered to be one of the most important steps in the retina manufacturing since any soldering flaws could cause an interruption of the electric field, resulting in an image with no meaning. For instance, if for an element, the centre wire of the coax touched the ground plane at the back side of the retina, that array element could become shorted to ground resulting in a completely out of work array element. Furthermore, if one of the cables became lose, no connection was attained and no signal could flow through the coaxial cable resulting in another fault.

As mentioned earlier, two different prototypes were designed and built for this thesis. The main factor that differentiates these two systems is the shape of their retina and their scanning (switching) method. The first system utilizes a cylindrical array of circular patch antennas while the other is a single column of patch antennas. As for the first system, array elements were printed on a flexible PCB so that it could be shaped into one third of a cylinder. Thus, a frame was designed so that the array was kept in a cylindrical form. Figure 4.2 represents the frame that was designed and manufactured for this specific purpose. As can be seen from this figure, the frame is made out of plastic which is a dielectric material to avoid reflection.

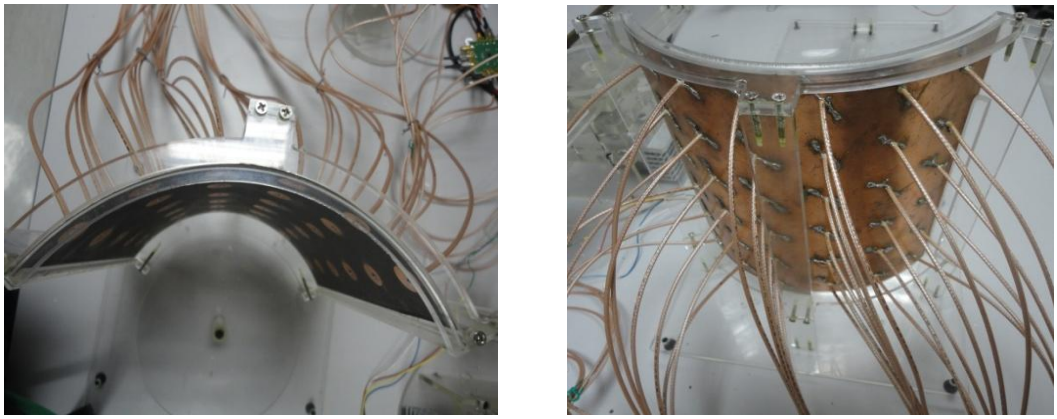

Figure 4.2 Frame made for holding cylindrical retina

The array of retina of the rotating imaging system was manufactured like that of the cylindrical array. However, it was located in a frame which kept it straight the whole time. Yet, the designed frame for this system was a bit more complex. To create a full view of the structure under inspection, the retina has to rotate and a motor is required. Thus, the designed frame was required to have a location for the motor in order to facilitate rotation of either the transmitting and receiving antennas or the

structure under test. As it was illustrated earlier, in Figure 3.13 and Figure 3.14, two possible frames could be fabricated for this retina; one with the motor at its base and one with the motor placed at the top. The common challenge concerning both schemes was the fact that by rotating the receiving and the transmitting units, different destructive noises could be introduced to the system. That is since the experiment is conducted in a normal laboratory environment with different instruments around the system rather than an anechoic chamber. Thus, with each rotation, the receiver faces a different direction and different reflections from the surroundings. Although attempts to reduce this problem by calibrating the system before each experiment were made, yet the reflections kept affecting the system. Moreover, the coaxial cables soldered to the antenna experience some movement with each rotation which causes the calibrations useless.

As explained in the previous chapter, it was decided to manufacture the rotating system which had no limitation on the height of the objects under inspection Figure 4.3. The frame was also designed in a way that it provided the system with the capability to either rotate the object or rotate the antennas. However, as for the results presented in this thesis, the system was configured such that the object was rotating while the antennas were kept stationary. This way the coaxial cables were fixed all the time and only one calibration is required.

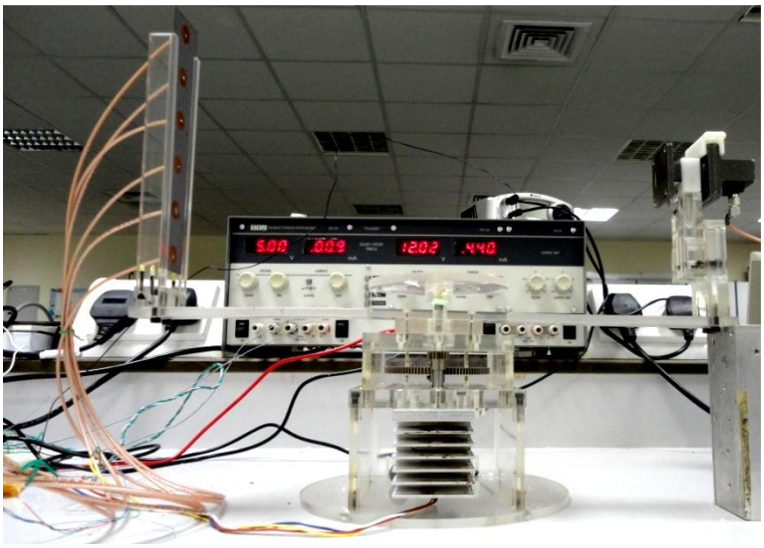

Figure 4.3 Frame of single column antenna array

4.2 Switch Network

Fabrication of the switching unit turned out to be the most time consuming part of this thesis. Moreover, the sensitivity of switches to electrostatic changes and handling the units was quiet challenging. Figure 4.4 provides an overview of this switch.

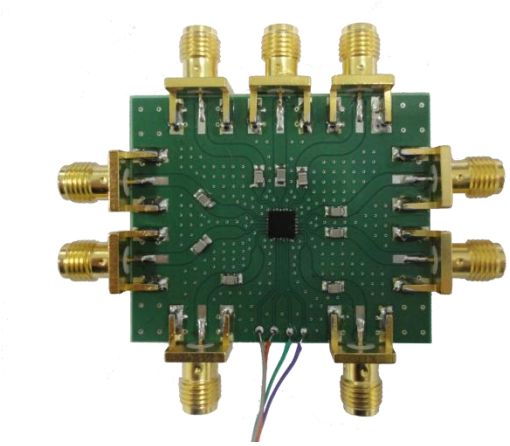

Figure 4.4 the designed SP8T switch

Furthermore, in case of cylindrical shape retina, due to the numerous cables and in order to keep the switches organized and to prevent any unnecessary movement, which could cause in need of system recalibration, a stand was designed and fabricated for the switches. This structure (Figure 4.5) helps keeping switches in a position where they could easily be moved while the chances of electrostatic shocks were reduced.

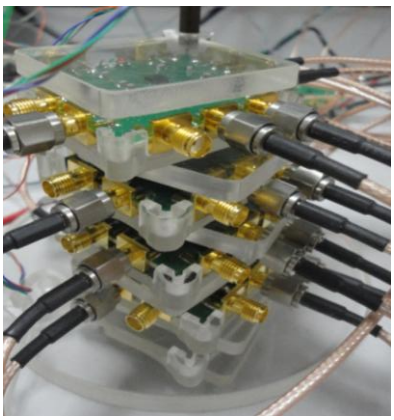

Figure 4.5 stand for the switches

4.3 Coding and Calibration

One of the most fundamental steps toward producing reliable results from the proposed microwave imaging system is to have a proper software and calibration method. MATLAB was chosen as the programming language to control the hardware and to process the data. One of the main reasons for using this software was its compatibility with the data acquisition card.

The MATLAB code developed for both retina configurations were written such that the effect of possible faults due to power variation of the sweep oscillator were eliminated. The MATLAB codes developed for these parts are presented in Appendix A parts c and d.

As mentioned earlier, calibration must be conducted before starting any measurements to establish common regions to all array elements. One common method to perform these calibrations in microwave imaging systems is to use a known object whose scattering pattern at all measurement positions is known. Using such a reference, and by comparing the expected field values with the actual values the weighting coefficients could be found[8].

Another method for calibration is to perform a set of measurements while no structures exist to scatter the electric field. Using this technique, the effect of possible reflections from the objects in the surrounding of the system can be eliminated. Furthermore, this technique eliminates possible variations in the received signal due to differences in antenna elements such as their soldering, cable length and etc.

4.4 Results

To test the performance of the system developed, two different prototypes were built; one with a quarter cylinder array comprising of 36 circular patch antenna elements and one a single column array of 6 circular patch elements. In order to test the performance of each, two prototypes were built and tested separately.

4.4.1 Cylindrical retina

In order to test the 36 element cylindrical system, a set of three Styrofoam cylinders of different sizes were first made to be used as opaque containers of

materials to be imaged. Figure 4.6 shows the setup and Styrofoam cylinders used for imaging the test objects.

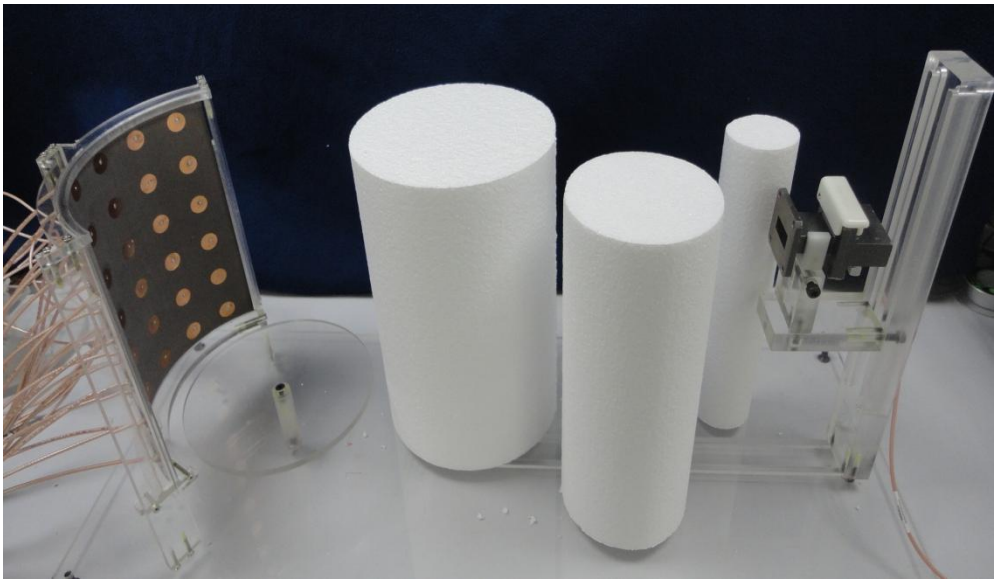

Figure 4.6 the cylindrical retina and Styrofoam cylinders

To start the testing process, first the system was calibrated to compensate for possible differences between the retina elements. Afterwards, a small metallic screw (as shown in Figure 4.7) was placed inside a Styrofoam cylinder and located in the test setup of Figure 4.6. Two images of the screw were obtained. The first image (upper image) shows a two dimensional representation and the other (the lower image) shows a three dimensional representation.

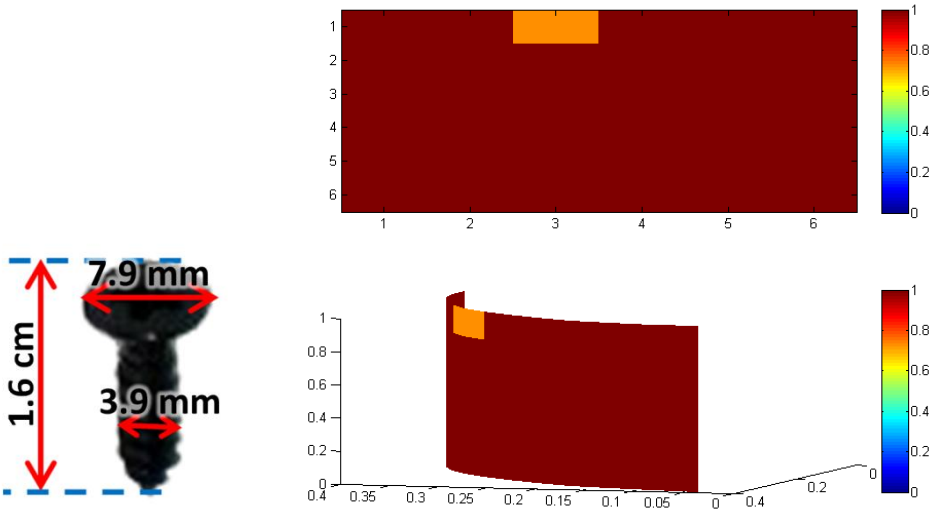

Figure 4.7 the screw and its image

As expected, the pixel representing the location where the screw existed in the Styrofoam has lower intensity compared to that of other pixels. However, the obtained image does not illustrate the shape of the screw since the system's resolution is not very high. To illustrate the effect of this low resolution, a small metallic plate (Figure 4.8) was placed in the Styrofoam cylinder and imaged. Figure 4.8 shows the image obtained for this test. Even though the physical size of the plate is larger than that of the screw, yet their images look similar with a minor difference in the intensity of their representing pixels.

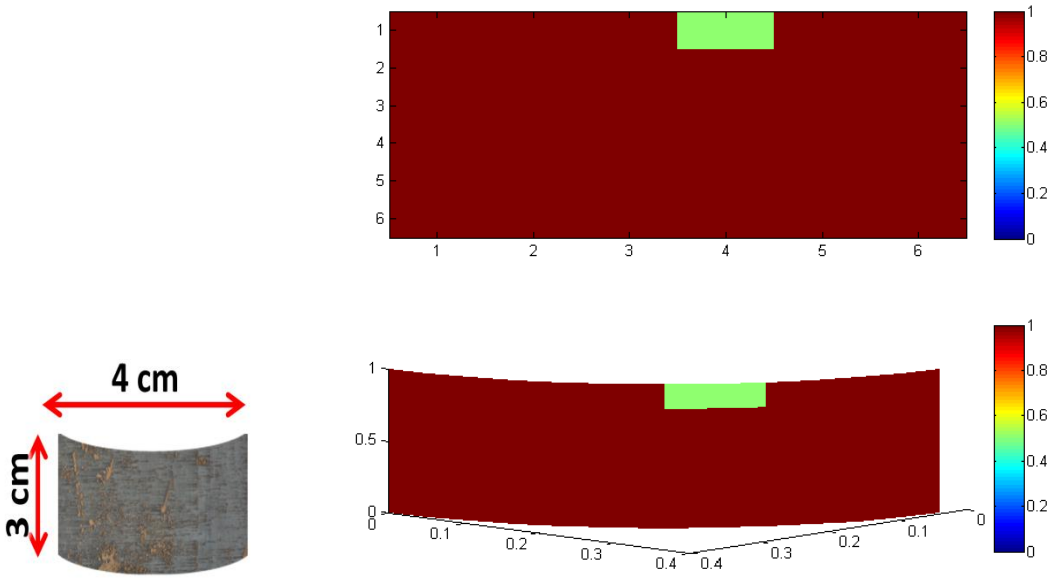

Figure 4.8 the metal plate and its image

To explain the relationship between the obtained image and the scanned structure, the model presented in Figure 4.9 can be used. Here, the size of each pixel, which is the area around each antenna element, is found using the distance between the neighboring array elements and their radius. This shows that each pixel of the obtained imaged using this system, represents dimensions of 3.38 cm by 3.38 cm.

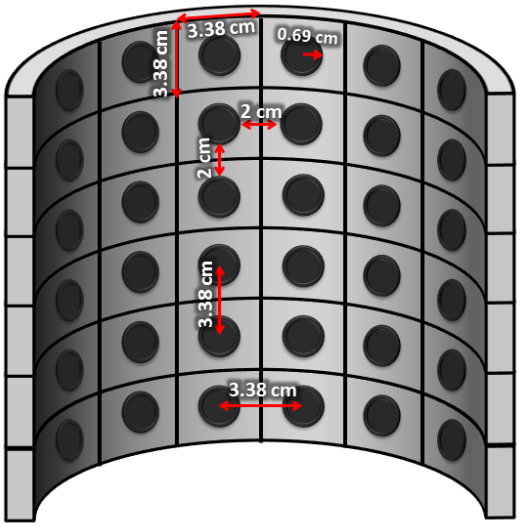

Figure 4.9 Antenna elements spacing and pixel size in cylindrical retina

Having this information, the acquired images using cylindrical retina can be compared in terms of their quality and accuracy against the dimensions of the structure under test. For instance, an approximation of the size of the screw from the first image, shown in Figure 4.7, can be calculated using the corresponding pixel size. Since the screw is occupying one pixel, the size from the image can be roughly estimated to be 3.38 cm x 3.38 cm, which is not precise. Meanwhile, the same estimation can be assumed for the image taken from the metallic plate which is closer to the actual size.

Despite the low physical resolution, there are a few methods that can be adopted to enhance the quality of the obtained image. Among all, the simplest is imaging the object of interest more than once, each time rotating it by an angle less than the spacing between two neighboring retina elements. At the end by superimposing the images on each other, a higher resolution image of the object under test can be obtained. Thus, the screw and metal plate were imaged twice with a 5 degree rotation for each object. The supper imposed images of this experiment are shown in Figure 4.10 (a) and (b).

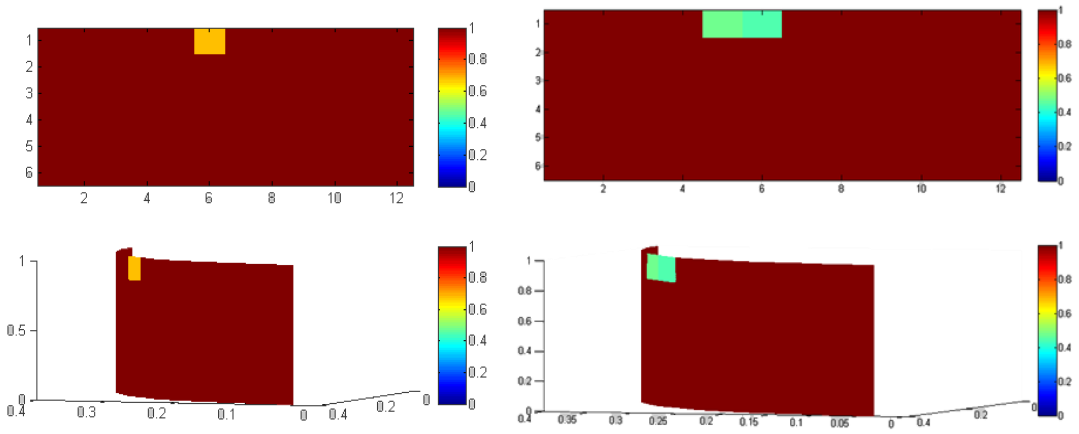

a) b)

Figure 4.10 the superimposed image of the screw (a) and the metallic plate (b)

Additionally, the size of the objects can be approximated as before using the new pixel dimensions which is reduced to 1.69 cm by 3.38 cm (Figure 4.11).

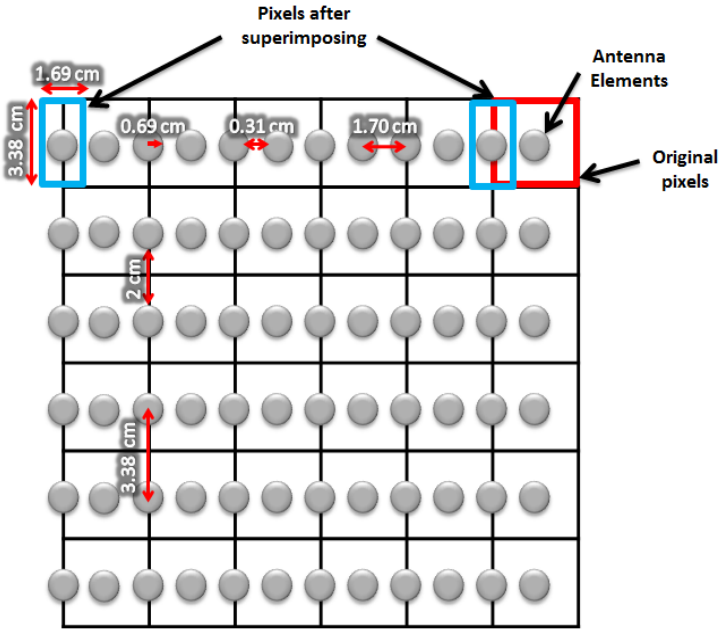

Figure 4.11 pixel size before and after superimposing

In Figure 4.11, the red square represents the pixel in the 36 element imaging system, while the blue square represent the new pixel size obtained by slightly rotating the structure and superimposing two images. Thus, the objects' size approximated from the images of Figure 4.10 is 3.38 cm (height) by 1.69 cm (width) and 3.38 cm by 5.07 for the screw and metallic plate, respectively. Even though the error in approximating the size of the metallic plate has increased and the shape of the

screw is not shown, yet the images of the objects are not similar anymore and, as can be seen from the figure, there is a clear indication of the size difference.

To test the performance of the system for objects of different dielectric properties, sizes and shapes, a wooden rod of 9.5 cm by 0.5 cm was scanned and as can be seen in Figure 4.12, due to its size, the intensity of pixels representing the wooden object is higher compared to that of the metallic screw; however, it has a lower intensity compared to the metallic plate.

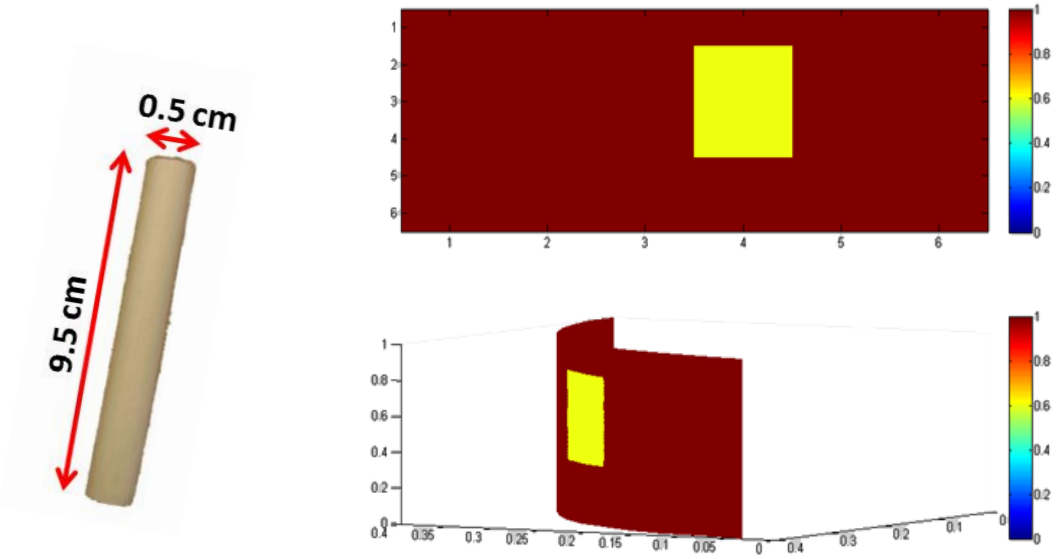

Figure 4.12 Wooden rod and its image

As can be seen in this figure, the image represents the wooden bar occupied 1 horizontal by 3 vertical pixels which represent a 3.38 cm by 10.14 cm object. The error in the width of this image is due to having the smallest pixel width of 3.38 cm.

As explained earlier, one of the main reasons for having a cylindrical microwave imaging system proposed was its benefits for imaging cylindrical structure compared to a planner system. To investigate the difference between the performance of the proposed system and a planner microwave imaging system, two tests were run.

As for the first setup (Figure 4.13 - a and b), a cylindrical aluminum object within a Styrofoam cylinder is placed in front of both a cylindrical and planer imaging system.

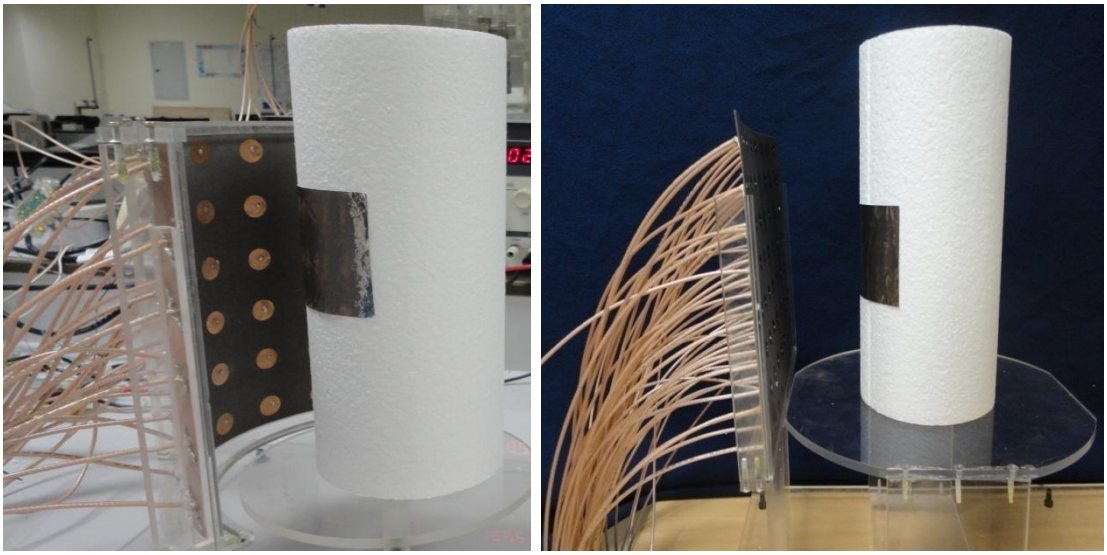

a) b)

Figure 4.13 imaging a cylindrical object by a) cylindrical retina, b) planner retina

Based on theoretical studies, it is expected to obtain a better image of the object with the cylindrical imaging system. Figure 4.14 (a) and (b) represent snapshots of images obtained from these systems respectively.

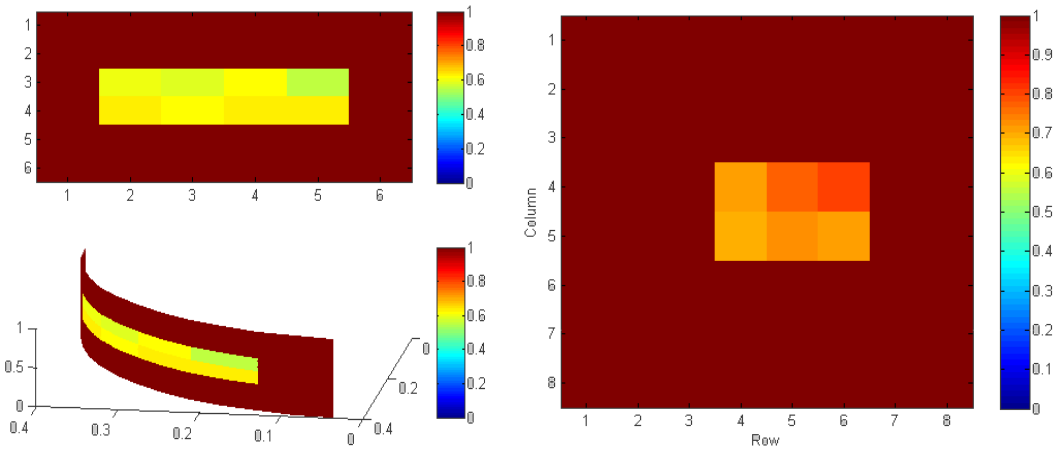

a) b)

Figure 4.14 Image of the curved aluminum foil obtained via (a) cylindrical and (b) planner imaging systems

As can be seen from these two figures, the image obtained via the cylindrical system (Figure 4.14 -a) is closer to the reality while the image obtained from planner system (Figure 4.14 -b) represents only a part of the object while half of it is not shown. The reason for this is that the spacing between the object and the array elements in the planer imaging system varies with respect to the array element's location while it is constant for the cylindrical system. Thus, when positioned at a

certain location between the transmitting and the receiving antennas, only one layer of the object could be imaged.

Even though the cylindrical system can work properly for cylindrical objects, yet when it comes to planner objects its performance is not as good as the planner imaging system. This is further illustrated by the images of Figure 4.15 (a) and (b) showing a planner aluminum foil placed in a cylindrical Styrofoam in front of cylindrical and planner retina.

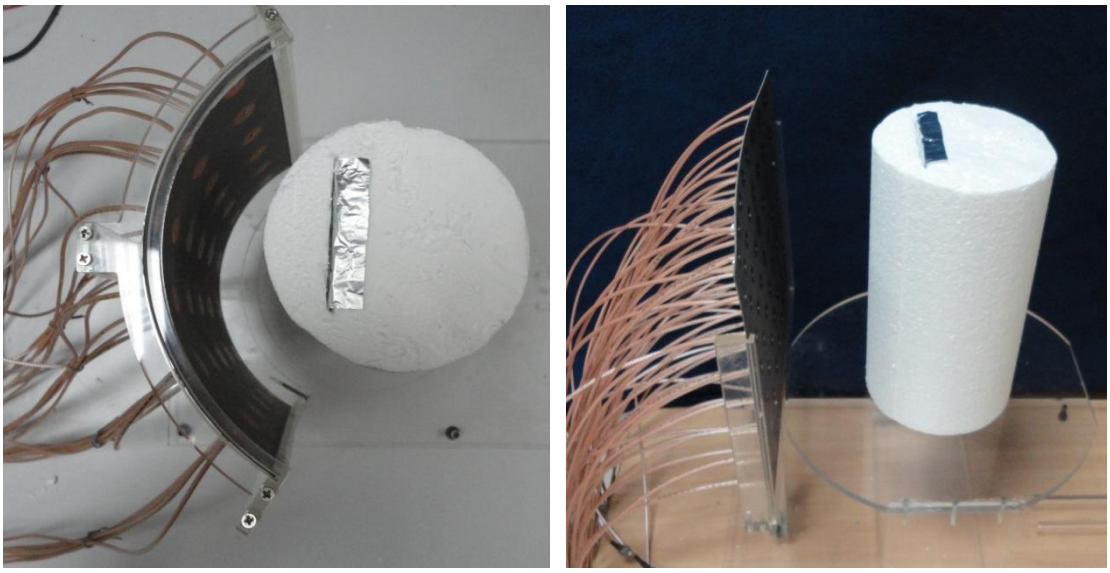

a) b)

Figure 4.15 imaging a planner item by a) cylindrical retina, b) planner retina

The images of Figure 4.16 (a) and (b) provide the results of this test; and as expected, the cylindrical system provides an image which is missing the center pixels due to the spacing of the object with respect to the retina. That is while this is not an issue for image obtained by planner a planner imaging system.

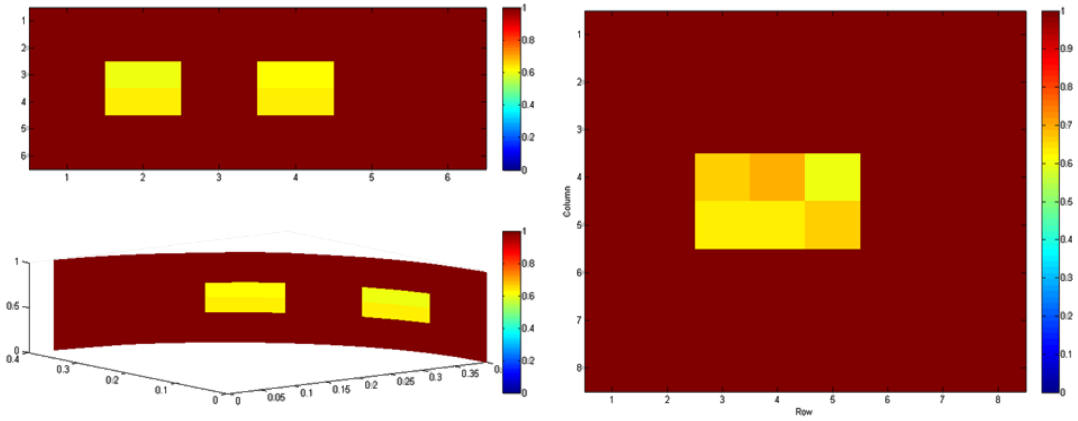

a) b)

Figure 4.16 Image of the flat aluminum foil obtained via (a) cylindrical and (b) planner imaging systems

4.4.2 Single column retina

To test the single column array imaging system, first the setup of Figure 4.3 was made. As can be seen from the figure, the illumination source is an open ended waveguide placed at one end while the receiving array is placed at the other end. The image of the object under investigation is obtained by scanning the object in a full 360^{o} rotation. Since the rotation step of the motor is adjustable, the horizontal resolution of the image can be easily increased or decreased. However, for testing purposes, the rotation angle was set to 30^{o}, providing a horizontal resolution of 12 pixels. That is while the vertical resolution is 6 pixels and is not variable. As can be seen in Figure 4.17 the pixel size in this case is 2.66 cm by 3.38 cm.

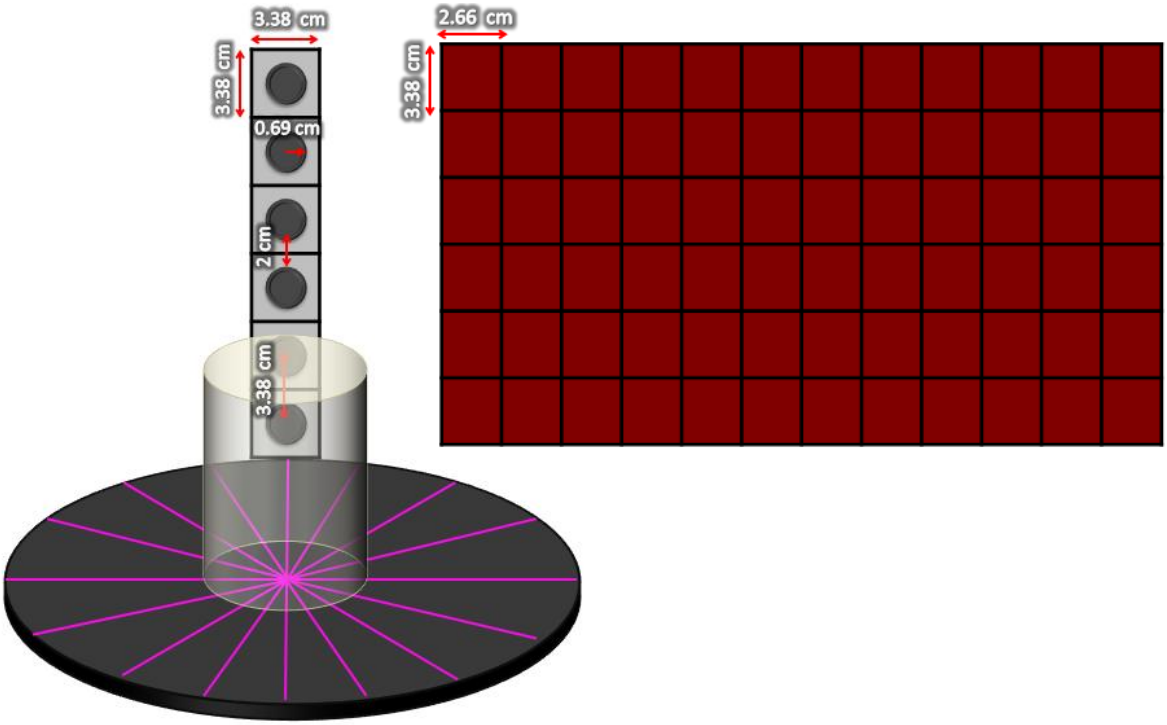

Figure 4.17 Antenna element's spacing and pixel size in moving retina when angel of rotation is set to be 30^{o}

Several experiments were conducted in order to test this system. The first test after calibration was imaging of a small metallic object within a Styrofoam. Thus, as for the previous part, the screw of Figure 4.7 was imaged and the obtained image is shown in Figure 4.18.

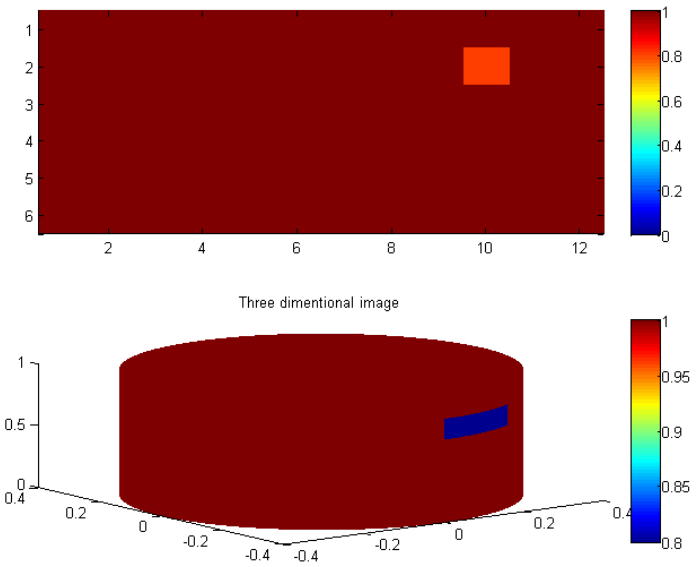

Figure 4.18 The image of screw inside the Styrofoam scanned by rotating retina

As that of Figure 4.7, the image of Figure 4.18 also illustrates the existence of the screw within a certain location of the Styrofoam cylinder. As can be seen, the shape of the screw is not visible; however, the image of the screw can be further illustrated if the rotation angle is decreased. Furthermore, the size of the screw approximated from this image is 3.38 cm by 2.66 cm while as shown in Figure 4.18 it is 1.6 cm by 0.79 cm.

As for the second test, a hexagonal wrench of dimension 7.3 cm by 3 cm by 0.3 cm, which basically can be explained as a small bent iron bar, was placed inside the Styrofoam and an image was obtained (Figure 4.19).

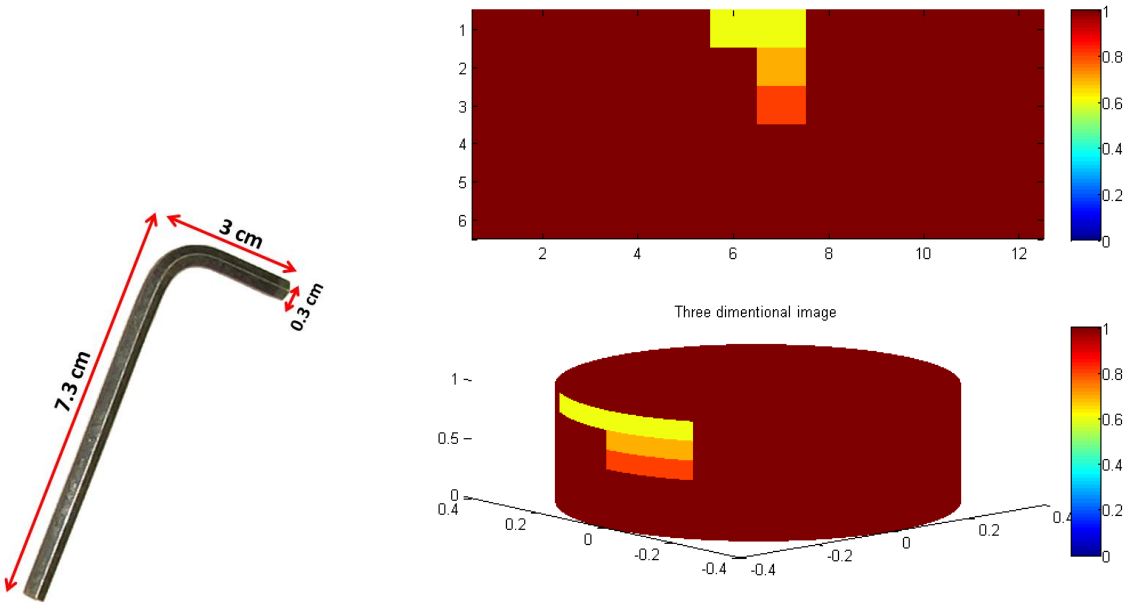

Figure 4.19 the image of hexagonal wrench

As seen in Figure 4.19, the hexagonal wrench is represented by 2 horizontal and 3 vertical pixels that give the size of 5.32 cm by 10.14 cm. In comparison with the real values there are some errors due to the placement of the wrench and the pixels sizes as illustrated by Figure 4.20.

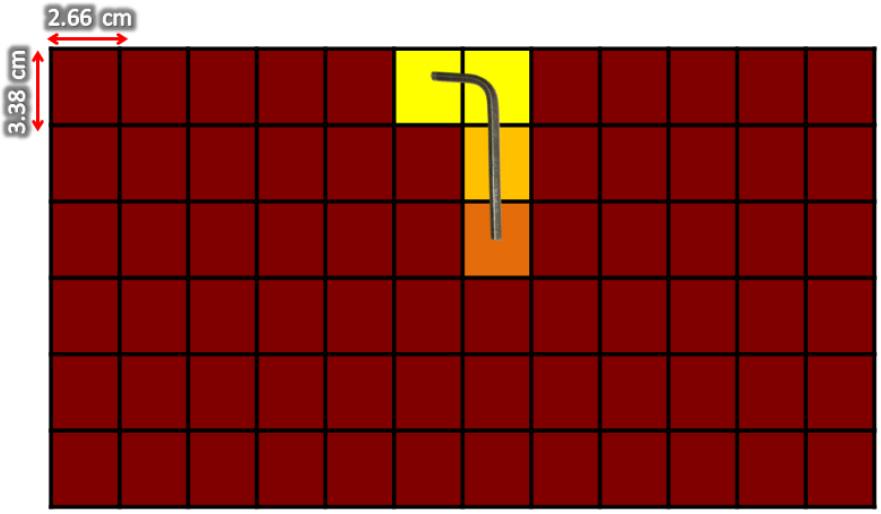

Figure 4.20 Placement of wrench

For the next step the system was tested using a half filled plastic bottle of water. Figure 4.21 illustrates the result obtained from this test. As can be observed from this image, the filled and empty parts of the bottle are completely distinguishable.

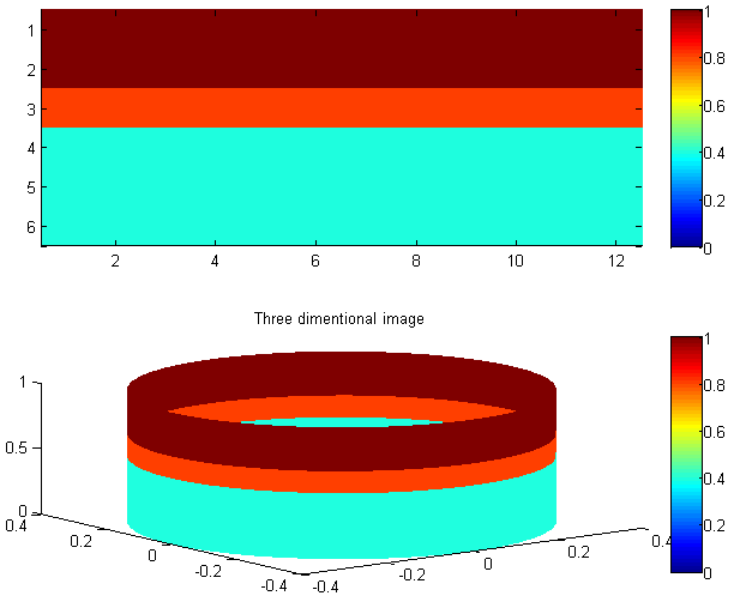

Figure 4.21 Image of a half filled bottle of water

To further examine this system, a screw was placed at a corner inside the bottle and the bottle was imaged. Figure 4.22 provides a snapshot of the image obtained for this scenario. As can be noticed from Figure 4.22, other than the pixel

element at location [6,10], there is another pixel next to it that demonstrates the existence of an impurity. The reason for this error is the rotation of the object. When the motor starts rotating, the object has inertia to stay at its first location. Furthermore, the water does not provide enough pressure to the screw to keep it from moving. Thus, whenever the motor moves, the object moves by a small amount resulting in such errors. This error can be fixed by either by rotating the antenna around the object rather than rotating the object, or fixing the object inside the water.

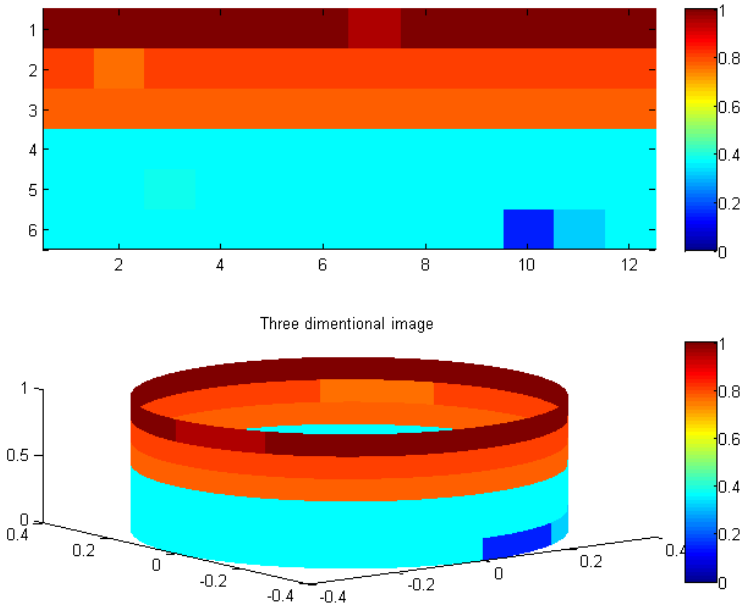

Figure 4.22 Image of a half filled bottle of water with a screw inside

CHAPTER 5

CONCLUSIONS AND FUTURE WORK

5.1 Conclusions

A microwave imaging system for cylindrical dielectric structures was proposed for which two different prototypes were designed, manufactured and tested. The two prototypes are distinguished from each other by the type of their receiving antenna and switching scheme. The cylindrical retina can obtain an image from one third of a cylindrical structure while the single column retina, which has the capability of rotating, can create a 360^{o} view of the structure under test. Although the vertical resolution for both retinas is the same, it was proven that a better horizontal resolution for rotating scheme can be achieved given the smaller degree of rotation. Moreover, the cylindrical retina, due to its fixed radius, can only image structures up to radius of 10 cm but in case of rotating retina there is more flexibility in terms of dimension of structure under test.

Both imaging schemes were tested for different structures of various size and material and they were able to successfully detect the impurities. Furthermore, a comparison between the system of cylindrical retina and a planner microwave imaging system was made. The test results highlight the advantage of cylindrical retina for imaging cylindrical structures as oppose to planner retina for imaging same structures.

5.2 Recommendations for Future Work

This system can be further improved to get a better quality of images and have better efficiency. This can be done by applying some changes to the current setup in terms of the receiving antenna array, the switching network and the image reconstruction scheme.

In terms of antenna retina, one possible way is to have loaded antenna that can reduce the coupling between the antenna elements and increase the quality of image.

Moreover, changing the type of antenna and replacing it with a bowtie antenna. The advantage of utilizing bowtie antennas is not only the fact that they can have smaller sizes for lower frequencies compared to other microstrip antennas but also the fact that they have wider bandwidth. The other solution is to have system that can work in multiple frequency range. This also can be covered by having bowtie antennas in system. Using multiple frequencies can improve the focusing effect and help to achieve a more detailed image of different layers of structure under test.

It is also advisable to adopt the reflection back scheme instead of through transmission and test it. It is possible that this can improve the overall result of the system since it uses only one antenna for both transmission and reception and the transmitted signal does not have to travel through entire body of the object and could result in more detailed result.

In the end, it is worth mentioning that although the proposed system is not appropriate for biomedical applications at its current stage, yet the system is designed in a way that can be easily altered to work at lower frequencies which are more appropriate for such applications. These applications are one of the main area of work that has been foreseen for this system's future practice.

REFERENCE LIST

[1] N. Petrovic, "Microwave Imaging of Biological Tissues," Elect. Eng. Dep., Univ Malardalen, 2007.

[2] R.Thadani. CAT Scan vs.MRI [Online]. Available: http://www.buzzle.com/articles/cat-scan-vs-mri.html

[3] Chua. *The Principles of Medical Ultrasound* [Online]. Available FTP: http://www.mrcophth.com/commonultrasoundcases/principlesofultrasound.html #advantages%20and%20disadvantages

[4] M. Miyakawa, "A study of the permittivity of biological tissues," Jpn.J. Hyperth. Oncol., vol. 4, pp. 306–315, 1988.

[5] P. Johnson, R. Chou, J. Lovberg, C. Martin. "passive microwave camera," International Journal of Infrared and Millimeter Waves, vol. 17, no. 7, pp. 1117-1138, July 1996.

[6] R.G. Reeves, A. Anson, D. Landen (eds), Manual Of Remote Sensing, Vol. 1, First Edition, Falls Church, 1975

[7] L. Jofre, M. Hawley, A. Broquetas, E. de los Reyes, M. Ferrando and A. Elias, "Medical imaging with a microwave tomographic scanner," IEEE Trans. Biomed. Eng., vol. 37, pp. 303–312, 1990.

[8] L. E. Larsen and J. H. Jacobi, "Microwave Scattering Parameter Imaging on an Isolated Canine Kidney," Medical Physics, Vol-6, pp. 394-403, 1979.

[9] M. Pastorino, "Microwave imaging," 1 ed., Hoboken, N.J.: John Wiley, 2010.

[10] Antoni Broquetas, Jordi Romeu, Juan M. Rius, Antonio R. Elias-Fuste, Angel Cardama, and Luis Jofre, "Cylindrical Geometry: A Further Step in Active Microwave Tomography," IEEE Trans. Microwave Theory Tech., vol. MTT-39, no. 5, pp. 836-844, May. 1991.

[11] T.Długosz, F.Ruan, D. Shi, Y. Gao, "Cylinder Model of Human Body Impedance Based on Proximity Effect", 3rd IEEE International Symposium on Microwavem Antenna, Propagation and EMC Technologies for Wireless Communications, 27-29 October 2009, Beijing, China, IEEE Conference Proceeding , ss 16-19.

[12] J.A. Richards, "Remote Sensing with Imaging Radar," Berlin, Germany: Springer, 2009.

[13] Y. J. Kim, L. Joffre, F. De Flaviis, and M. Q. Feng, "3D Microwave imaging technology for damage detection in concrete structures," presented at Proceedings of the International Symposium on Smart Structures and Materials SPIE, Long Beach, 2003.

[14] M.T. Ghasr, “Real-time and portable microwave imaging system,” Ph.D. dissertation, Dept. Elect. Eng., Missouri univ. of science and technology, 2009.

[15] J. Ch. Bolomey, H. de Talhou¨et, and Y. Anguill, “Mise en service et test de deux cam´eras microondes pour applications biom´edicales,” Proc´edure GBM/TEP no. 84012, Contrat ANVAR no. A844735, 1986.

[16] S. Y. Semenov, R. H. Svenson, and A. E. Boulyshev, A. E. Souvorov,V. Y. Borisov, Y. Sizor, A. N. Starostin, K. R. Dezern, G. P. Tatsis, andV. Y. Baranov, “Microwave tomography: Two-dimensional system forbiological imaging,” IEEE Trans. Biomed. Eng., vol. 43, pp. 869–877,1996.

[17] P. M. Meaney, M. W. Fanning, D. Li, S. P. Poplack and K. D. Paulsen, “A Clinical Prototype for Active Microwave Imaging of the Breast,” IEEE Transactions on Mircorwave Theory and Techniques, Vol-48, No. 11, pp. 1841–1853,November 2000.

[18] Paul M. Meaney, Margaret W. Fanning, Dun Li, Steven P. Poplack, and Keith D. Paulsen, “A clinical prototype for active microwave imaging of the breast,” IEEE Transactions on Microwave Theory and Techniques, Volume 48, Issue 11, Part 1, Nov. 2000 Page(s):1841 – 1853.

[19] M. Harwood (2010, 01). Whole Body Imaging [Online]. Available FTP: http://www.securitymanagement.com/news/faqs-whole-body-imaging-006637

[20] C.A. Balanis, Antenna theory: analysis and design , 3rd ed. Hoboken, New Jersey: Wiley & Sons Inc , 2005.

[21] P. J. Bevelacqua. (2010). Field Regions [Online]. Available FTP: http://www.antenna-theory.com/basics/fieldRegions.php

[22] A.J. Jundi,“NEAR-FIELD FMCW RADAR FOR MAPPING OF MULTILAYER STRUCTURES”, Master’s thesis, American University of Sharjah, 2010.

[23] H. Lee, Z. Liu, Y. Xiong, C. Sun, X. Zhang, "Design, fabrication and characterization of a Far-field Superlens",Solid State Communication, 146, 202, 2008

[24] M. Bertero and C. De Mol, E. Wolf, "Super-resolution by data inversion", Progress in Optics, vol. XXXVI, pp.129 - 178 , 1996. : Elsevier

[25] S. K. Lehman, "Superresolution Planar Diffraction Tomography through Evanescent Fields," International Journal of Imaging Systems & Technology, 12(1), pp16–26, 2002.

[26] R. A. Day. (2009). *Near Field Imaging* [Online]. Available FTP: http://www.xdcr.com/stm.html

[27] M. Fernando, K. Busawon, M. Elsdon, and D. Smith, "Fundamental issues in antenna design for microwave medical imaging applications," Proceeding of the 7th Symposium on Communication Systems, Networks and Digital Signal Processing 2010, pp. 869-874, Newcastle upon Tyne, UK, July 2010

[28] A. Joisel, J. Mallorqui, A. Broquetas, J. M. Geffrin, N. Joachimowicz, M.V. Iossera, L. Jofre and J. -C. Bolomey, "Microwave Imaging Techniques for Biomedical Applications," Instrumentation and Measurement Technology Conference, 1999.

[29] A. Broquetas, J. Romeu, J. M. Rius, A. R. Elias-Fuste, A. Cardama and L.Jofre, "Cylindrical Geometry: A Further Step in Active Microwave Tomography,"IEEE Transactions on Mircorwave Theory and Techniques, Vol-39, No.5, pp. 836–844, May 1991.

[30] S. Y. Semenov, R. H. Svenson, A. E. Boulyshev, A. E. Souvorov, V. Y. Borisov, Y. Sizov, A. N. Starostin, K. R. Dezern, G. P. Tatsis and V. Y. Baranov,"Microwave Tomography: Two-Dimensional System for Biomedical Imaging,"IEEE Transactions on Biomedical Engineering, Vol-43, No. 9, pp. 869–877,September 1996.

[31] P. M. Meaney, K. D. Paulsen and J. T. Chang, "Near-Field Microwave Imaging of Biologically-Based Materials Using a Monopole Trenceiver System," IEEE Transactions on Mircorwave Theory and Techniques, Vol-46, No. 1, pp. 31–43, January 1998.

[32] D. Li, P. M. Meaney, T. Raynolds, S. A. Pendergrass, M. W. Fanning and K. D.Paulsen, "A BROADBAND MICROWAVE BREAST IMAGING SYSTEM," 2003 IEEE 29th Annual Biomedical Conference, Proceeding of, pp. 83–84, Mars 2003.

[33] Y.Huang and K.Boyle, Antennas: From Theory to Practice. Hoboken, NJ: Wiley, 2008.

[34] R. J. Mailloux, *Phased Array Antenna Handbook*, 2nd edition. Boston, MA: Artech House INC, 2005.

[35] T.F.Lai, W. N. L. Mahadi & N. Soin, "Circular Patch Microstrip Array Antenna for KU-Band", WCSET 2008 Conference, Bangkok, Thailand.

[36] E.Rufus, Z.C,Alex, and PV.Chaitanya, 'A modified Bow-Tie Antenna for Microwave Imaging Applications',115-122, Journal of Microwaves, Optoelectronics and Electromagnetic Applications, Vol. 7, No. 2, December 2008

[37] S. W. J. Chung, R. A. Abd-Alhameed, P. S. Excell, C. H. See, D. Zhou and J G Gardiner, Resistively Loaded Wire Bow-tie Antenna for Microwave Imaging By Means of Genetic Algorithms

[38] Merriam-Webster Dictionary (2010).*Tomography* [Online]. Available FTP: http://www.merriam-webster.com

[39] A. C. Kak and Malcolm Slaney, Principles of Computerized Tomographic Imaging, Society of Industrial and Applied Mathematics, 2001.

[40] V. Barthes and G. Vasseur, "An inverse problem for electromagnetic prospection, in Applied Inverse Problems, P. C. Sabatier, Ed. Berlin: Springer-Verlag, 1978.

[41] M. Slaney and A. C. Kak, "Imaging with diffraction tomography," TR-EE 85-5, School of Electrical Engineering, Purdue Univ., Lafayette, IN, 1985.

Appendix A

MATLAB codes

a)Circular Patch

In this part, the MATLAB code for circular patch antenna calculations and radiation pattern is presented. Some parts of this code were taken from [20].

```
clc;clear;
freq=7.5;
Zin=50;
h=0.254;
er=2.2;
lt=0.0004;
con=59.6*10^6;
lambda_o=30.0/freq;
ko=2*pi/lambda_o;%free space wavenumber
F=8.791/(freq*sqrt(er));
a=F/sqrt(1+2*h/(pi*er*F)*(log(pi*F/(2*h))+1.7726));%The physical
radious
ae=a*sqrt(1+2*h/(pi*er*a)*(log(pi*a/(2*h))+1.7726));%The effective
radious
t=[0:0.001:pi/2];
x=ko*ae*sin(t);
j0=besselj(0,x);
j2=besselj(2,x);
j02p=j0-j2;
j02=j0+j2;
grad=(ko*ae)^2/480*sum((j02p.^2+(cos(t)).^2.*j02.^2).*sin(t).*0.001);
emo=1;
m=1;
mu0=4*pi*10^(-7);
k=ko*sqrt(er);
stop=0;
gc=emo*pi*(pi*mu0*freq*10^9)^(-3/2)*((k*ae)^2-
m^2)/(4*(h/100)^2*sqrt(con));

gd=emo*lt*((k*ae)^2-m^2)/(4*mu0*h/100*freq*10^9);

gt=grad+gc+gd;%total conductance
Rin0=1/gt;
temp1=Zin/Rin0*besselj(1,k*ae)^2;
maxrho=ae;
minrho=0;
tempk=1;
while tempk>0.00001
    nk=0;
    rhox=linspace(minrho,maxrho,100);
    temp=besselj(1,k.*rhox).^2;
    for kk=1:99
        if temp(kk)-temp1<=0
            if temp(kk+1)-temp1>0
                nk=nk+1;
                minrho=rhox(kk);
                maxrho=rhox(kk+1);
```

```
            end
        else
            if temp(kk+1)-temp1<=0
                nk=nk+1;
                maxrho=rhox(kk);
                minrho=rhox(kk+1);
            end
        end
    end
    [tempk,kk]=min(abs(temp-temp1));
    RHOo=rhox(kk);
end
%Calculating the directivity of the patch
th=0:90; phi=0:360;
[t,p]=meshgrid(th.*pi/180,phi.*pi/180);
x=sin(t).*ko.*ae;
J0=besselj(0,x); J2=besselj(2,x);
J02P=J0-J2; J02=J0+J2;
Ucirc=(J02P.*cos(p)).^2 + (J02.*cos(t).*sin(p)).^2;
Umax=max(max(Ucirc));
Ua=Ucirc.*sin(t).*(pi./180).^2;
Prad=sum(sum(Ua));
D=4.*pi.*Umax./Prad;
DdB=10.*log10(D);
% Plots of Radiation Patterns
% Normalized radiated field
%         E-plane and H-plane patterns : 0 < th < 90
th=0:90; thr=th.*pi./180;
x=sin(thr).*ko.*ae;
J0=besselj(0,x);
J2=besselj(2,x);
Eth1=J0-J2;
Eph1=(J0+J2).*cos(thr);

Eth2=20.*log10(Eth1./max(Eth1));
Eph2=20.*log10(Eph1./max(Eph1));
Eth2(Eth2<=-60)=-60;
Eph2(Eph2<=-60)=-60;

Eth(1:91)=Eth2(1:91); Eth(91:270)=Eth2(91); Eth(271:361)=Eth2(91:-
1:1);
Eph(1:91)=Eph2(1:91); Eph(91:270)=Eph2(91); Eph(271:361)=Eph2(91:-
1:1);

phi=0:360;
hli1=plot(-90:90,[fliplr(Eth2) Eth2(2:end)],'b-');
set(gca,'position',[0.13 0.11 0.775 0.8]);
h1=gca; h2=copyobj(h1,gcf); axis([-90 90 -60 0]);
set(h1,'xcolor',[0 0 1]); set(hli1,'erasemode','xor');
hx=xlabel('\theta (degrees)','fontsize',12);

axes(h2); hli2=plot(-90:90,[fliplr(Eph2) Eph2(2:end)],'r:'); axis([-
90 90 -60 0]);
set(h2,'xaxislocation','top','xcolor',[1 0 0]);
set([hli1 hli2],'linewidth',2);
legend([hli1 hli2],{'E_{\theta} (E-plane)','E_{\phi} (H-plane)'},4);
xlabel('\theta (degrees)','fontsize',12);
```

b) The antenna elements cross talk

```
clear
clc
lambda=3e8/.75e10;
R=lambda/20:lambda/20:lambda;    % range of antenna element spacings
syms Gt Gr
patch_rad=1.3716e-2;
Rcm=R*100;
arc=Rcm;                    %elements physical spacing on the retina
r=3*21/(2*pi);              %21 is the length of the square retina
theta=arc/r;
Dh=sqrt(2*r^2-2*r^2*cos(theta));
Dv=Rcm;                              %elements vertical distance
D_v(1,:)=Dh;          %distance vector
D_v(2,:)=Dv;
DL=2.5e-2;                          %transmitter antennas largest
dimention
d_far=2*DL^2/lambda;                %calculating the farfield of the
transmitter
R1=d_far+10e-2;                     %Distance between the transmitter and
the reciever

pt1=10^(10/10)/1000;                %Radiated power from the transmitter
(in watts)
pr1=(lambda/(4*pi*R1))^2*pt1;       %Maximum power recieved by the center
array element

Pref=pr1*0:pr1/100:pr1*1;           %Reflection coefficient vector

for j=1:2
    %calculating the coupled power for different reflected powers
    %(Horizental and Vertical elements)
    for i=1:101;
        pr(j,i,:)=(lambda./(4.*pi.*D_v(j,:))).^2.*Pref(i);
    end
    figure(j)
        title ('Coupled power from a single element')
    ylabel ('Coupled power (dBm)')
    if j==1
        xlabel ('Horizental Distance (Cm)');
    else

         xlabel ('Vertical Distance (Cm)');
    end

    hold on
    for k=2:4:101;
        F(k,:)=10*log(pr(j,k,:)*1000);
        plot(R*100,F(k,:))
    end
end
figure (3)
hold on
for i=1:4:101;
    F(i,:)=10*log([2*pr(1,i,:)+2*pr(2,i,:)]*1000);
    plot(R*100,F(i,:))
    xlabel ('Distance (Cm)');
    ylabel ('Coupled power (dB)')
```

```
    title ('Coupled power from first tire of elements')
end
```

c) The code for imaging system with 36 element antenna

```
clear;clc;
%Opening the analog device and channels
if (~isempty(daqfind))
    stop(daqfind);
end
data=0;
Result=zeros(6,6);
Rez_norm=zeros(6,6);
% Infinit loop for obtaining real time images
while (1)
    Result=zeros(6,6);
    Rez_norm=zeros(6,6);
    for (j=1:6);
        AI = analoginput('nidaq','Dev1');%the device and its ID
        chan= addchannel(AI,3);% channel allocation
        SampleRate = 200; %200 samples per second
        duration = 0.25; %0.25 second acquisition
        set(AI,'SampleRate',SampleRate)
        ActualRate = get(AI,'SampleRate');
        set(AI,'SamplesPerTrigger',duration*ActualRate)
        blocksize = get(AI,'SamplesPerTrigger');
        AI.InputType = 'SingleEnded';
        Fs = ActualRate;
        % Gathering the data from the DAQ for all the elements of a
row
        for (i=0:5)
            dio = digitalio('nidaq','Dev1');
            addline(dio,0:2,'out');
            data=i;
            bvdata = dec2binvec(data,3);
            putvalue(dio,bvdata);
            putvalue(dio.Line(1:3),bvdata);
            % Getting the data
            start(AI)
            wait(AI,duration + 0.1)
            Data = getdata(AI);
            Result(i+1,j)=abs(sum(Data)/SampleRate);
            delete(dio)
            clear dio
        end
        delete(AI)
        clear AI
        % The calibration matrix
        test_=[
        0.1267    0.1032    0.1477    0.1315    0.1775    0.0543
        0.1267    0.1032    0.1477    0.1315    0.1775    0.0543
        0.1267    0.1032    0.1477    0.1315    0.1775    0.0543
        0.1267    0.1032    0.1477    0.1315    0.1775    0.0543
        0.1267    0.1032    0.1477    0.1315    0.1775    0.0543
        0.1267    0.1032    0.1477    0.1315    0.1775    0.0543 ];
```

```
        Rez_norm(:,j)=roundn((Result(:,j))./(test_(j,:)'),-2);
        % Rounding the normalized data up to decrease the effect of
input
        % variations
        for (l=1:6);
            if (Rez_norm (l,j)>1)
                Rez_norm(l,j)=1;
            end
        end
        Rez_norm = ceil (Rez_norm*10)/10;

      %   Plotting the image
        subplot(2,1,1);
        imagesc(Rez_norm,[0 1]);colormap(jet);colorbar;shg
        subplot(2,1,2);

        % Generating a quarter of a cylinder
        [x,y,z] = cylinder( 0.4,51);
        [m,n] = size(z);
        xx = zeros(m,n/4);
        yy = ones(m,n/4);
        zz = zeros(m,n/4);
        for k=1:m
            for p=1:n/4
                xx(k,p) = x(k,p);
                yy(k,p) = y(k,p);
                zz(k,p) = z(k,p);
            end;
        end;
        %Plotting the data
        colormap(jet);
        surface(xx,yy,zz,'FaceColor','texturemap',…
            'EdgeColor','none','Cdata',flipud(Rez_norm))
        colorbar;
        view(3)
    end
end
```

d) The code for imaging system with rotating antenna

```
%outputing signal
clear;clc;
%Open the analog device and channels
if (~isempty(daqfind))
    stop(daqfind);
end
data=0;
Result=zeros(6,12);
Rez_norm=zeros(6,12);
for (j=1:12);

    AI = analoginput('nidaq','Dev1');%the device and its ID
    chan= addchannel(AI,3);%channel allocation
    SampleRate = 100;
```

```
duration = 0.25; %1 second acquisition
set(AI,'SampleRate',SampleRate)
ActualRate = get(AI,'SampleRate');
set(AI,'SamplesPerTrigger',duration*ActualRate)
blocksize = get(AI,'SamplesPerTrigger');
AI.InputType = 'SingleEnded';

Fs = ActualRate;
for (i=0:5);
    dio = digitalio('nidaq','Dev1');
    addline(dio,0:2,'out');
    data=i;
    bvdata = dec2binvec(data,3);
    putvalue(dio,bvdata);
    putvalue(dio.Line(1:3),bvdata);
    %input data
    start(AI)
    wait(AI,duration + 0.1)
    Data = getdata(AI);
    Result(i+1,j)=abs(sum(Data)/SampleRate);
    delete(dio)
    clear dio
end
delete(AI)
clear AI
%outputing signal
%Adjusting the rotation direction
dio = digitalio('nidaq','Dev1');
addline(dio,0:3,'out');
data1=Direction_;
bvdata1 = dec2binvec(data1,4);
putvalue(dio,bvdata1);
putvalue(dio.Line(1:4),bvdata1);
%Open the analog device and channels
AO = analogoutput('nidaq','Dev1');
chan = addchannel(AO,1);
f=490;
%Set the sample rate and how long the data will be sent
duration = 0.25;
f=f*duration;
SampleRate = f*5;
set(AO,'SampleRate',SampleRate)
set(AO,'TriggerType','Manual')
NumSamples = SampleRate*duration;
% Create a signal that we would like to send, 500 Hz sin wave
x = linspace(0,2*pi,NumSamples);
%the motor drive requires a pulse train to work
data= 2+5*square(f*x,10)';
% Put the data in the buffer, start the device, and trigger
putdata(AO,data)
start(AO)
trigger(AO)

% clean up, close down
wait(AO,duration+0.1)

data1=0;
delete(dio)
clear dio
delete(AO)
clear AO
```

```
    test_=[
    0.2254     0.1893     0.1417     0.1414     0.2688     0.1599
    0.2254     0.1893     0.1417     0.1414     0.2688     0.1599
    0.2254     0.1893     0.1417     0.1414     0.2688     0.1599
    0.2254     0.1893     0.1417     0.1414     0.2688     0.1599
    0.2254     0.1893     0.1417     0.1414     0.2688     0.1599
    0.2254     0.1893     0.1417     0.1414     0.2688     0.1599
    0.2254     0.1893     0.1417     0.1414     0.2688     0.1599
    0.2254     0.1893     0.1417     0.1414     0.2688     0.1599
    0.2254     0.1893     0.1417     0.1414     0.2688     0.1599
    0.2254     0.1893     0.1417     0.1414     0.2688     0.1599
    0.2254     0.1893     0.1417     0.1414     0.2688     0.1599
    0.2254     0.1893     0.1417     0.1414     0.2688     0.1599 ];

    Rez_norm(:,j)=roundn((Result(:,j))./(test_(j,:)'),-2);

%     Rounding up the numbers within a range

    for (l=1:6);
        if (Rez_norm (l,j)>1)
            Rez_norm(l,j)= 1;
        end
    end
        Rez_norm = ceil (Rez_norm*10)/10;

        subplot(2,1,1);
    imagesc(Rez_norm,[0 1]);colormap(jet);colorbar;shg
    subplot(2,1,2)
    colormap(jet)
    [x,y,z] = cylinder(0.4,50);
    surface(x,y,z, 'FaceColor','texturemap','EdgeColor',...
            'none','Cdata',flipud(Rez_norm))
    colorbar;
    view(3)
end
```

Appendix B

Image reconstruction mathematical algorithm

Microwave signals considered diffractive, this research deals with tomographic imaging with diffracting sources[39].One of the main obstacles in such imaging is the effects of reflections and diffractions. Moreover, most of the structures that are examined in microwave imaging are inhomogeneous, so to represent electromagnetic waves the general equation (0.1) can be used.

$$[\nabla^2 + k(\overrightarrow{r})^2]u(\vec{r}) = 0 \tag{0.1}$$

By ignoring the effect of polarization equation (0.2):

$$K(\vec{r}) = k_0 n(\vec{r}) = k_0[1 + n_\delta(\vec{r})] \tag{0.2}$$

where,

$K(\vec{r})$ is refractive index of medium

K_0 is the average wave number of the medium

n($\vec{r}$)is electromagnetic refractive index of media

$n_\delta(\vec{r})$ is the refractive index deviations (since object has finite size this index is zero outside the object)

Therefore equation (0.2) can be rewritten as equation (0.3)

$$\left(\nabla^2 + {k_0}^2\right)u(\vec{r}) = -{k_0}^2[n(\vec{r})^2 - 1](\vec{r})u(\vec{r}) \tag{0.3}$$

Where n($\vec{r}$) is given by equation (0.4).

$$n(\vec{r}) = \sqrt{\frac{u(\vec{r})\epsilon(\vec{r})}{u_0\epsilon_0}} \tag{0.4}$$

where,

u = magnetic permeability/ u_0 magnetic permeability average value

ϵ = dielectric constant/ ϵ_0 dielectric constant average value

Now, assuming equation(0.5) and(0.6)

$$O(\vec{r}) = {k_0}^2[n(\vec{r})^2 - 1] \tag{0.5}$$

$$u(\vec{r}) = u_0(\vec{r}) + u_s(\vec{r}) \tag{0.6}$$

Where,
$u(\vec{r})$ = total field
$u_0(\vec{r})$= incident field (the field present without any inhomogeneities)
$u_s(\vec{r})$ = scattered field (this is the only part of total field that can be attributed only to the inhomogeneities)

By using equation (0.5), having inhomogeneous situation in hand, equation (0.1) can be rewrite as equation (0.7).

$$\left(\nabla^2 + {k_0}^2\right)u_s(\vec{r}) = -O(\vec{r})u(\vec{r}) \tag{0.7}$$

To solve the above scalar equation (Helmholtz equation) for $u_s(\vec{r})$ Green's function (equation (0.8) should be used.

$$\left(\nabla^2 + {k_0}^2\right)g\left(\vec{r}\middle|\vec{\acute{r}}\right) = -\delta(\vec{r} - \vec{\acute{r}}) \tag{0.8}$$

Since the green's function, $g\left(\vec{r}\middle|\vec{\acute{r}}\right)$ is only function of $\vec{r} - \vec{\acute{r}}$ it can present as g($\vec{r} - \vec{\acute{r}}$) [39],[40].So now the solution of equation(0.7)can be shown as equation (0.9);

$$u_s(\vec{r}) = \int g(\vec{r} - \vec{\acute{r}})O(\vec{\acute{r}})u(\vec{\acute{r}})d\vec{\acute{r}} \tag{0.9}$$

Now, to find the solution of equation (0.6), the Born approximation, which is a well known equation specially for circular shape antennas, is used. Here, the equation (0.9) is written as

$$u_s(\vec{r}) = \int g(\vec{r} - \vec{r}')O(\vec{r}')u_0(\vec{r}')d\vec{r}' + \int g(\vec{r} - \vec{r}')O(\vec{r}')u_s(\vec{r}')d\vec{r}' \tag{0.10}$$

If the scattered field, is small compare to incident field the second integral can be ignored and the result will be as shown in equation (0.11).

$$u_s(\vec{r}) \approx u_B(\vec{r}) = \int g(\vec{r} - \vec{r}')O(\vec{r}')u_0(\vec{r}')d\vec{r}' \tag{0.11}$$

In general the ith order Born field can be represented by equation (0.12)

$$u_B{}^{(i+1)}(\vec{r}) = \int g(\vec{r} - \vec{r}')O(\vec{r}')[u_0(\vec{r}') + u_B(\vec{r}')]d\vec{r}' \tag{0.12}$$

After expanding the equation (0.12)the approximate expression for scattered field, u_B, is found to be

$$u_B{}^{i}(\vec{r}) = \sum_{j=0}^{i} u_j(\vec{r}) \tag{0.13}$$

Equation (0.13) shows the result for first order born approximation, which represents the first order scattered field. Therefore, in general, it can be said that each part of a structure produces a partial scattering field, which are interacting with other scattering centers in the object [39][40].Therefore, having a converging Born series can give the total field as the sum of the partial scattered field. A very important condition (equation (0.14)) for using Born approximation is to have a scattered field smaller than incident field

$$u_0(\vec{r}) > u_s(\vec{r}) \tag{0.14}$$

Having an inhomogeneous cylinder, which is the assumed situation in this research, this condition can be written in terms of size of the object and refractive

index. In such a case the field inside the object can be approximated by equation (0.15).

$$u_{object}(\vec{r}) = Ae^{jk_0(1+n_\delta)\vec{s}\,.\vec{r}} \tag{0.15}$$

Where, $\vec{s}$ is the unit vector presenting the direction of propagation of the incident wave $u_0(\vec{r})$.

In this situation, where the wave is propagating through the structure, the phase shift through structure can be estimated by the equation (0.16):

$$4\pi n_\delta \frac{a}{\lambda} \tag{0.16}$$

where,
λ is the wavelength of incident field
a is radius of cylinder
$n_\delta(\vec{r})$ is the refractive index deviations

VITA

Soudeh Heydari Nasab was born on April 1983, in the city of Kerman in Iran. Later, when she was 5 years old, she moved to Tehran with her family where she completed her studies up to college. After 2 years of working in Tehran in an electrical engineering company, she decided to complete her studies and moved to UAE. She started her undergraduate studies in spring 2005 at the American university of Sharjah and finished it in 2009 with a B.Sc. degree in Electrical Engineering. As a part of her undergraduate studies, she participated in a research on RF Signal Harvesting for which she co-authored three IEEE conference proceedings and one peer reviewed journal paper. Right after her graduation, she started her master degree studies at the same university, American University of Sharjah, and obtained her M.Sc. certificate in June 2011.